

Single-Particle Theory of Fission*

A. BRANDT

Department of Applied Mathematics, Weizmann Institute, Rehovot, Israel

AND

I. KELSON†

Wright Nuclear Structure Laboratory, Yale University, New Haven, Connecticut 06520

(Received 10 September 1968; revised manuscript received 6 December 1968)

The single-particle aspects of nuclear fission theories are investigated. The liquid drop model is shown to be essentially equivalent to an independent particle model with the requirement that particles occupy the lowest orbits. The consequences of relaxing this requirement are pursued and are shown to be significant. A natural framework is provided in which the mass asymmetry of fission arises naturally. A report is given of the technical aspects and the quantitative results of a detailed model calculation. Some of the indicated conclusions are formulated as phenomenological rules.

I. INTRODUCTION

THE phenomenon of fission involves the dividing of the atomic nucleus into two (or more) parts, and was first observed experimentally in the late thirties.¹ The occurrence of such a division for the heavier elements is simply dictated by energy considerations.² A large amount of energy may be released in the process, because of the smaller binding energy per nucleon for these nuclei.

The characteristics of fission, as well as of all other properties of the nucleus, and the processes which it may undergo, are, in principle, determined by a many-body Hamiltonian H . Although there is no conclusive experimental evidence either way, it is customary to ascribe to this Hamiltonian the form

$$H = \sum_i K_i + \sum_{i < j} V_{ij}. \quad (1)$$

K is a one-body operator, including the kinetic energy term, the spin-orbit interaction and perhaps other terms. The two-body operator V represents an interaction between different nucleons, which, in principle, can be determined (or at least closely investigated) from scattering data of nucleons on nucleons, and from information about the bound-state structure of the two-nucleon system (namely, the deuteron).³ The reconstruction of such an operator is indeed the subject of the efforts of a few groups of investigators. Perhaps, the most comprehensive is that of Breit. The knowledge of the exact form of the Hamiltonian is still only part of the problem. It needs to be solved. In particular, we expect the fissioning of specific nuclei to be described by a time-dependent solution of this many-body problem. The overwhelming complexities of this problem call for drastic approximations to be made. When one deals with

properties related to *structure* and simple scattering processes of a given nucleus, the usual approximations involve a limitation of the number of particles considered and a truncation of the space of states which they are allowed to populate. This is based on the fact that such properties indeed depend only on the degrees of freedom of the last few so-called "active" nucleons.⁴ The bulk of the nucleus, the core, plays the role of an essentially inert, uninvolved observer. In the truncated space, the original Hamiltonian is modified, serving as an "effective" interaction. However, since the precise form of the transition

$$H_{\text{real}}(\text{Complete Problem}) \rightarrow H_{\text{eff}}(\text{Truncated Problem})$$

is not clear, one may consider H_{eff} as a starting point, and treat it through a set of primary parameters to be fitted to the experiment. This, in fact, has been the underlying philosophy of the shell model,⁵ which has scored a great many successes in the field of nuclear spectroscopy. The inherent calculational difficulties still present in the shell model, along with the discovery of rotational spectra, led to the development of the collective model of nuclei.⁶ In this model, it is impossible to distinguish between "active" and "passive" nucleons. Rather, all nucleons participate, in comparable measure, in the motion which the model describes. Hence the term collective. The reduction in the number of degrees of freedom comes about by altogether disposing of the individual degrees of freedom of the nucleons, and replacing them by some variables which relate to the nucleus as a whole. The structure of the nucleus is determined by an over-all *equilibrium* shape (which is permanently deformed for rotational nuclei) and by *small variations* relative to it (giving rise to vibrational spectra). The relation between the shell model and the collective model, the ways in which they complement each other, and through which they can be integrated into a unified model,

* Work supported in part by the U.S. Atomic Energy Commission Contract No. AT(30-1)-3223.

† Present Address: Department of Physics and Astronomy, Tel Aviv University, Tel Aviv, Israel.

¹ O. Hahn and F. Strassmann, *Naturwiss.* **27**, 11 (1939); **27**, 89 (1939).

² It nevertheless was not realized fully until *after* the discovery of fission.

³ G. Briet, *Rev. Mod. Phys.* **34**, 766 (1962).

⁴ This idea is a direct carryover from atomic physics.

⁵ A general reference is A. de-Shalit and I. Talmi, *Nuclear Shell Theory* (Academic Press Inc., New York, 1963).

⁶ A. Bohr and B. R. Mottelson, *Kgl. Danske Videnskab. Selskab, Mat.-Fys. Medd.* **27**, No. 16 (1953).

have been the subject of thorough investigation in the past decade. One may safely say that, at present, we possess, through these two models, a fairly comprehensive and, to a large extent, quantitative understanding of low-energy nuclear structure and reactions.

Yet, both models are incapable of providing a meaningful framework for the treatment of fission. In fission, clearly, we are confronted with a radical rearrangement of *all* the nucleons in the system, and hence the shell model (and in particular the *spherical* shell model) is inapplicable. As for the collective model, it treats basically *small* variations in the nuclear shape, whereas the fission process clearly involves much larger and more elaborate variations. It is perhaps because of the inapplicability of the major nuclear models that the study of fission has become rather isolated from the rest of nuclear physics.

The first (and so far dominant) model to deal with fission is the liquid drop model (LDM).⁷ From a historical, as well as conceptual, point of view, it preceded the collective model and paved the road for it. Superficially, they are almost identical, inasmuch as the nucleus is described by some collective coordinates which pertain to its over-all shape. The nucleus is described as a drop of homogeneous, homogeneously charged, incompressible, nonviscous, sharply bounded liquid, which is subject to an irrotational, hydrodynamical flow. Of all these characterizations of the problem which one replaces the original Hamiltonian with, none is truly essential. The basic feature is that the *instantaneous over-all shape of the nucleus plays the role of dynamic variable*. With the particular assumptions stated above, as well as with a much wider class of assumptions, the geometrical nuclear surface is in itself sufficient. The potential-energy part of the Hamiltonian is composed of an electrostatic and a nuclear interaction. The electrostatic term is simply and classically given by a double volume integral over the nuclear charge density

$$V_{\text{els}} \sim \iint_{\text{Nucel}} \frac{\rho(\mathbf{r}_1)\rho(\mathbf{r}_2)}{|\mathbf{r}_1 - \mathbf{r}_2|} d^3r_1 d^3r_2. \quad (2)$$

The nuclear energy is itself a sum of two terms, one proportional to the volume and the other proportional to the surface of the nucleus:

$$V_{\text{Nucel}} = C_{\text{Vol}} \times \text{Vol} + C_{\text{Sur}} \times \text{Sur}. \quad (3)$$

However, with the assumption of incompressibility of nuclear matter, the volume energy simply becomes an additive constant which contributes nothing to the dynamics of the system and can be altogether left out of the discussion. The origin of this form is in the Bethe-Weizsäcker semiempirical mass formula, where these two terms represent an expansion of the binding energy in powers of $A^{-1/3}$. It is quite clear that the extrapolation of this form into shapes which are grossly

distorted is fraught with serious dangers. Nevertheless, the liquid drop model (LDM), in its basic, simple form has been responsible for providing a great deal of insight into the fission process. The static, and more recently dynamic, consequences of it were investigated in great detail by Wheeler and collaborators,⁸ and by Swiatecki and collaborators.⁹ In fact, in the last 15 years, many of the significant theoretical studies were either carried out or initiated by the latter.¹⁰

The role of the single particles in the nucleus, and their Fermi-Dirac nature, was a central question from the start in the understanding and the theory of fission. The LDM, inasmuch as it is a microscopic analog of a macroscopic liquid, is basically a many-particle model, where the particles have a mean free path much *smaller* than the dimensions of the total system. This is in a rather sharp contradiction with our current general picture of nuclear structure, which maintains that nucleons have a *long* mean free path, reflecting the exclusion principle in nuclear matter. As a matter of fact, this very consideration has been critically discussed by Bohr and Wheeler, at the very inception of the LDM. More recent studies (including the present one) showed that this contradiction has a minor effect, at most. It turns out, with a surprising degree of generality, that an extreme *independent* particle model (with simple assumptions) reproduces the LDM nuclear surface energy. Thus, it would seem, the LDM may be used as it was originally conceived, although its motivational basis is altered. Experimentally there were various observations,¹¹ related in particular to the different fission characteristics of even and of odd nuclei as evidence for the single-particle nature of nuclei undergoing fission. A quantitative analysis of the process based on a single particle approach was performed by Nilsson.¹² The Nilsson single-particle model¹³ has enjoyed tremendous success in nuclear-structure theory, and is also applied to the theory of fission. In some respects the present work may be viewed as an extension of the former. In particular, the nuclear shapes discussed in the present work are more general in nature, and are more characteristic of the fission process.

Before proceeding with the exposition of ideas, the presentation of results, and their analysis, we must make one point extremely clear. The present work does *not* constitute an independent, self-sufficient model of fission. Rather, it is an attempt to illuminate (quantitatively as well as qualitatively) various aspects and concepts in relation to other existing models. It is

⁸ D. L. Hill and J. A. Wheeler, Phys. Rev. **89**, 1102 (1953).
⁹ S. Cohen and W. J. Swiatecki, Ann Phys. N.Y. **22**, 406 (1963); J. R. Nix and W. J. Swiatecki, Nucl. Phys. **71**, 1 (1965); W. J. Swiatecki, Phys. Rev. **104**, 993 (1956).

¹⁰ This is also the case for the present work.

¹¹ V. M. Strutinskii, Zh. Eksperim. i Teor. Fiz. **45**, 1841 (1963) [English transl.: Soviet Phys.—JETP **18**, 1298 (1964)].

¹² S. G. Nilsson (private communication).

¹³ S. G. Nilsson, Kgl. Danske. Videnskab. Selskab, Mat.-Fys. Medd. **29**, No. 16 (1955).

⁷ N. Bohr and J. A. Wheeler, Phys. Rev. **56**, 426 (1939).

hoped that a better understanding of such aspects will eventually pave the way to a rigorous, integrated theory of nuclear fission.

II. COLLECTIVE- AND SINGLE-PARTICLE DEGREES OF FREEDOM

As was already pointed out, the description of the nucleus in terms of the coordinates of the individual nucleons is a formidable undertaking. Attempts to construct a framework which will forego the use of these numerous coordinates and will concentrate on a much smaller number of degrees of freedom serve a dual purpose. First, the computational complexities may be reduced to a workable level; and second, the new coordinates may be more closely related to our intuitive picture of the fissioning nucleus and to the physical observables which the process involves.

The basic problem, therefore, involves the transcription of a Hamiltonian $H(\mathbf{r}_1, \dots, \mathbf{r}_A; \dot{\mathbf{r}}_1, \dots, \dot{\mathbf{r}}_A)$ dependent on the coordinates and their derivatives of the A nucleons (as well as on their spin and isospin) into a Hamiltonian $H(\xi_1, \dots, \xi_n; \dot{\xi}_1, \dots, \dot{\xi}_n)$ which depends on some set of variables (ξ_1, \dots, ξ_n) and their derivatives. It is assumed throughout the following discussion that $H(\{\mathbf{r}\}; \{\dot{\mathbf{r}}\})$ is precisely known, though in reality this is not the case. Nevertheless, enough of its basic characteristics are well understood. In particular, when no velocity-dependent forces are taken into account, H may be simply separated into a kinetic term which depends *only* on the derivatives of the coordinates, $T(\{\dot{\mathbf{r}}\})$, and a potential term which depends only on the coordinates themselves— $V(\{\mathbf{r}\})$.

If the set of “collective” variables $\{\xi\}$ ($\xi_i; i=1, \dots, n$) corresponds to some rearrangement (say, a linear transformation) of the individual variables—particularly meaning that there is no reduction in the *number* of independent variables—then the transformation simply generates a different, but basically equivalent way of describing the A -body system. Although such a procedure may have its merits, it is hard to see how it will reduce the enormity of the task at hand. Clearly, then, before constructing H , the first step is the proper selection of the “collective” coordinates. This selection is effectively a truncation of the configuration space, and as such must be guided by physical considerations. If this truncation corresponds to some region of configuration space to which the system is in actuality confined, then the Hamiltonian H can be simply mapped over into H on the truncated space. This, however, is generally uncertain, and we have no way of checking it in practice, anyway. Thus, the effective truncation must be accompanied by a certain modification of the Hamiltonian as well. At this point of the reasoning one may be tempted to drop altogether the many-body Hamiltonian, and to use the “effective” Hamiltonian $\hat{H}(\{\xi\})$ as a starting point. That, indeed, is what the LDM does. The

variables describe a shape which defines the boundary of a liquidlike nuclear matter. The *potential*-energy part of H has the simple form of a sum of Coulomb electrostatic energy, and nuclear-surface energy. On the other hand, the dependence of the kinetic energy term on $\{\dot{\xi}\}$ and perhaps also on $\{\xi\}$ themselves, is more complicated. One must incorporate further assumptions about the nature of the internal motion,¹⁴ and resort, in most cases, to elaborate hydrodynamical descriptions. As we shall see, the question of the counterpart to the kinetic-energy term in the many-body Hamiltonian, is persisting in other treatments as well.

The many-body Hamiltonian, in second quantization notation, has the form

$$H = \sum_{\alpha, \beta} \langle \alpha | K | \beta \rangle a_{\alpha}^{\dagger} a_{\beta} + \frac{1}{4} \sum_{\alpha, \beta; \gamma, \delta} \langle \alpha \beta | V | \gamma \delta \rangle a_{\alpha}^{\dagger} a_{\beta}^{\dagger} a_{\delta} a_{\gamma}. \quad (4)$$

The creation and annihilation operators a_{α}^{\dagger} , a_{β} create and annihilate single-particle states, and thus construct a description directly in configuration (or momentum) space. In some problems in nuclear structure, the collective coordinates (such as relate to the total quadrupole moment) are considered *in addition* to the particle coordinates. In such cases they are redundant, and special arguments must be advanced as to why the resulting treatment may still be basically valid.¹⁵ Generally, however, conditions must be imposed to cut down the redundancy thus introduced. If the conditions are physically acceptable and mathematically manageable, then not only is the redundancy removed, but a prescription may be provided for constructing the effective Hamiltonian, \hat{H} , which depends on the collective variables only.

The most widely used approach¹⁶ to the choice of collective variables very much resembles that of the LDM. It essentially specifies—not necessarily completely—the *total* nuclear spatial density $\rho(\mathbf{r})$. The basic feature of nuclear matter—its incompressibility—is introduced *a priori* by limiting the acceptable $\rho(\mathbf{r})$ to those functions which describe a standard constant density, or ones that fluctuate around it. Once the standard density is fixed (with proper allowance for surface diffuseness) all that remains to be done, is to specify the region in space to which the nucleus is confined. This can be done, as the LDM would do, by describing through the variables (ξ_1, \dots, ξ_n) the two-dimensional surface which forms the nuclear boundary.

An alternative method may be employed, which relates the new coordinates directly to the Hamiltonian H . The central argument is that the nucleus can be described as a system of *independent* particles, moving

¹⁴ J. A. Wheeler (unpublished work).

¹⁵ S. A. Moszkowski, Phys. Rev. **103**, 1328 (1956).

¹⁶ S. A. Moszkowski, in *Handbuch der Physik*, edited by S. Flugge (Julius Springer-Verlag, Berlin, 1957), Vol. 39, p. 411.

in some common average single-particle potential. In particular, the ground state would thus be described by

$$\phi_0 = \prod_{\lambda=1}^A a_{\lambda}^{\dagger} | 0 \rangle = \mathcal{A}(\varphi_1 \varphi_2 \cdots \varphi_A), \quad (5)$$

where a_{λ}^{\dagger} creates a single-particle state φ_{λ} with appropriate quantum numbers (such as j , m_j , τ_z etc.) out of the vacuum $| 0 \rangle$. The properties of ϕ_0 are determined through a variational principle demanding that

$$\langle \phi_0 | H | \phi_0 \rangle = \min \quad (6)$$

or

$$\delta \langle \phi_0 | H | \phi_0 \rangle = 0 \quad (7)$$

with ϕ_0 assumed to be kept normalized and antisymmetrized.

This variational principle gives rise to the familiar Hartree-Fock theory of atomic and nuclear structure.¹⁷ To recap briefly, the states $\varphi_1, \cdots, \varphi_A$ which are the occupied orbits making up ϕ_0 , are to be eigenstates of the Hartree-Fock one-body operator h ,

$$h\varphi_{\lambda} = \epsilon_{\lambda}\varphi_{\lambda}. \quad (8)$$

On the other hand, h is related to its own eigenstates through

$$h = \sum_{\alpha, \beta} \{ \langle \alpha | K | \beta \rangle + \sum_{\lambda} \langle \alpha \lambda | V | \beta \lambda \rangle \} a_{\alpha}^{\dagger} a_{\beta}. \quad (9)$$

These equations have to be solved simultaneously in a self-consistent manner. If the variation is unrestricted, one obtains ϕ_0 which is an approximation to the ground state, with an expectation value

$$E_0 \equiv \langle \phi_0 | H | \phi_0 \rangle = \frac{1}{2} \langle \phi_0 | K + h | \phi_0 \rangle. \quad (10)$$

Now let $\Omega_1, \Omega_2, \cdots, \Omega_n$ be a set of one-body operators which relate directly to the nuclear-density distribution. These may be, for example, a series of multipole operators, or combinations of them. This specific set of operators has a set of expectation values in the approximate ground state ϕ_0 which we define as

$$\xi_i^{(0)} = \langle \phi_0 | \Omega_i | \phi_0 \rangle. \quad (11)$$

There is clearly a correspondence between *any* state ψ of the nucleus (expressed, say, in configuration space) and a set of numbers $\{\xi\}$ through

$$\xi_i = \langle \psi | \Omega_i | \psi \rangle. \quad (12)$$

This will only be a one-to-one correspondence if $\{\xi\}$ form a complete set of variables. Generally, however, there will be many states corresponding to the same set of values $\{\xi\}$. To lift this ambiguity as much as possible, we extend in a natural way the variational approach of the Hartree-Fock theory. Again, we limit ourselves to antisymmetrized, normalized product wave func-

tions. Of all states ϕ satisfying (11), we select that one $\phi(\{\xi\})$ for which $\langle \phi(\{\xi\}) | H | \phi(\{\xi\}) \rangle$ is smallest. This is equivalent to solving the variational problem with (11) as a subsidiary condition, and, in practice, is simply done by the use of Lagrange multipliers.

Thus, the expectation value $\langle \phi(\{\xi\}) | H | \phi(\{\xi\}) \rangle$ provides a unique value at each generalized point $\{\xi\}$, and is further usually associated with a unique state in configuration space. The physical meaning of this procedure may be understood as follows: Assume that the system is restricted (by some external force, say) to have the set of expectation values $\{\xi\}$ and is maintained long enough under this restriction so that it is allowed to attain as low an energy as possible. The lowest energy is then identified as the *potential-energy term* of the Hamiltonian. Clearly, by hypothetically substituting in the Hamiltonian \hat{H} , $\{\xi\} = 0$ one would be simply left with this *potential-energy* term, and, in fact, a good deal can be learned about the system merely by inspecting the potential surface. It must be emphasized, though, that in it we do include a great deal of the *kinetic energy* of the *individual* nucleons, as is evident by forming the expectation value of the many-body Hamiltonian H .

The construction of a kinetic term, namely one that depends on the time derivatives of the generalized coordinates, is much more elaborate in this framework. If we assume, as is customarily done, that the kinetic energy is a bilinear function of the form

$$T = \sum_{i, j=1}^n m_{ij} \dot{\xi}_i \dot{\xi}_j, \quad (13)$$

then the problem reduces to the extraction of the "mass parameters" m_{ij} which themselves may be functions of $\{\xi\}$.

In practice, the performance of the self-consistency program, using a realistic many-body Hamiltonian, is far too complicated. For two-body interactions which have a hard core, one runs immediately into divergences in the calculation of matrix elements between unmodified single-particle states. In fact, the construction of a one-body average field is impossible, and one must introduce strong many-particle correlations to counteract the hard-core effect. This very difficulty persists to some extent, even for interactions which have so-called "soft" or "soft-hard" cores.

The procedure that is followed alleviates the necessity of going through the self-consistency problem, simply by *postulating* what is the solution to this problem. This does not mean that the conceptual significance of an average potential, and its relation to the many-particle Hamiltonian are abandoned. It merely represents the elimination, through lack of choice, of an intermediate numerical step. One must hope that the results are not affected considerably, and that no appreciable physical insight is lost. Since the immediate, rigorous relation to the original Hamiltonian is not

¹⁷ For a general exposition, see F. Villars, in *International School of Physics "Enrico Fermi" Course XXIII*, edited by V. F. Weisskopf (Academic Press Inc., N.Y., 1963).

apparent, one must also specify an effective, residual two-body interaction, operative between states of the new single-particle field. This new, effective Hamiltonian is then used to produce the collective Hamiltonian which depends on the new coordinates.

A case in hand for such a procedure is the nuclear shell model. The average single-particle potential is *spherical*, usually a harmonic oscillator or a Saxon-Woods type, with a strong spin-orbit coupling. The residual two-body interaction is either standardized (as a Gaussian or Yukawa) or treated as variable and fitted to experimental data. An extremely successful extension of this approach to nonspherical shapes is provided by the Nilsson model.¹³ Here, again, the emphasis is on the description of the average potential, in this case a quadrupole deformed harmonic oscillator, while the residual two-body interaction is usually taken on an *ad hoc* basis.

The extension of these ideas to any arbitrary shape is straightforward. Let the variables $\{\xi\}$ define any shape $S\{\xi\}$ which in turn uniquely defines a one-body potential $h\{\xi\}$. This potential generates a spectrum of single-particle wave functions

$$h\{\xi\}\varphi_\lambda\{\xi\} = \epsilon_\lambda\{\xi\}\varphi_\lambda\{\xi\}. \quad (14)$$

If care is taken to reproduce the average nuclear density, then the incompressibility of nuclear matter is automatically taken into account. In practice, this is equivalent to a simple restriction on the spatial extension of the field $h\{\xi\}$.

The first-order identification of the nuclear energy (as distinct from the Coulomb energy) as a function of $\{\xi\}$ is obtained by simply summing up the energies of the individual nucleons

$$E_{N\text{ucl}}\{\xi\} = \sum_{\lambda=1}^A \epsilon_\lambda\{\xi\} = \langle \phi\{\xi\} | h\{\xi\} | \phi\{\xi\} \rangle, \quad (15)$$

where $\phi\{\xi\}$ is the normalized, antisymmetrized product wave-function of the states $\varphi_\lambda\{\xi\}$; $\lambda=1, \dots, A$. This simple expression is *not* identical to any of the proper expressions discussed above, and its application requires some justification.

Our basic argument is that any part of the potential energy which depends only on the total number of particles (or, equivalently, on the nuclear volume) can be left out safely from the analysis of the fission process. Furthermore, all *residual* terms (namely, nuclear terms which do depend on the shape) need only be known up to a proportionality constant, which may in turn be adjusted separately to observed data.

First, we note that the single-particle energies in the Hartree-Fock potential already include a good deal of the two-body interaction. Upon varying the depth of the potential by a constant (fixing the Fermi level of nuclear matter), we add a term of the form

$$\Delta E_{N\text{ucl}} = \sum_{\lambda=1}^A \epsilon_f = A \epsilon_f \quad (16)$$

which is independent of the shape. Next, we consider the types of *residual interaction* $V_{\text{Res}}(\mathbf{r}_1, \mathbf{r}_2)$ which we might add to the summation of Eq. (15). The expectation value added may be expressed:

$$\langle \phi\{\xi\} | V_{\text{Res}} | \phi\{\xi\} \rangle = \sum_{\lambda > \mu}^A \langle \varphi_\lambda \varphi_\mu | V_{\text{Res}} | \varphi_\lambda \varphi_\mu \rangle. \quad (17)$$

If we follow a common argumentation and consider V_{Res} to be a very *short-range* interaction (zero range in the limit) we notice that the matrix elements have the form

$$\langle \varphi_\lambda \varphi_\mu | V_{\text{Res}} | \varphi_\lambda \varphi_\mu \rangle = \int d\mathbf{r}_1 d\mathbf{r}_2 \varphi_\lambda^*(\mathbf{r}_1) \varphi_\mu^*(\mathbf{r}_2) \times V^{TS} \delta(\mathbf{r}_1 - \mathbf{r}_2) \{ \varphi_\lambda(\mathbf{r}_1) \varphi_\mu(\mathbf{r}_2) - \varphi_\mu(\mathbf{r}_1) \varphi_\lambda(\mathbf{r}_2) \}, \quad (18)$$

where V^{TS} depends only on the spin-isospin degrees of freedom and the integration is understood to include a summation over those as well. A similar consideration applies to the pairing force¹⁸ as well, rendering the result *independent of the shape* of the average field. Having defined the average potential associated with each "point" $\{\xi\}$ we still have a choice in deciding which particular levels will be occupied by the A nucleons of the system. It is true that to be a solution to the strict minimizing problem of Eq. (6) the configuration of A nucleons must be composed of the energetically lowest levels. However, as written in Eq. (7), the extremum equation gives rise to numerous solutions, some of which are only *local* energy minima and some of which are saddle points of the energy surface $\langle \phi | H | \phi \rangle$. We simulate each such solution as a different configuration of levels in the standard $h(\{\xi\})$ rather than solve for the modified average potential. This is done both for mathematical and computational simplicity, and because an element of arbitrariness in the construction of the average field has already been introduced. It must be borne in mind, though, that the actual increment of energy resulting in the rearrangement will thus be usually smaller than might be expected from a mere inspection of the levels of $h\{\xi\}$. We shall not explicitly take this particular effect into account because of the lack of a rigorous quantitative handle on it.

The first rule of level occupation that one naturally tries is the one mentioned above; namely, the lowest-energy levels. In anticipation of results that follow, we may state with a large degree of generality that with this prescription the LDM potential-energy surface is essentially reproduced. This may provide partial justification for defining the LDM potential surface as the one generated by this particular approach.

That this prescription is indeed somewhat arbitrary, was hinted at above. The potential energy as it is defined here already contains a considerable amount of *kinetic* energy of individual nucleons. Why, then,

¹⁸ L. S. Kisslinger and R. A. Sorenson, Kgl. Danske Videnskab. Selskab, Mat.-Fys. Medd. **32**, No. 9 (1960).

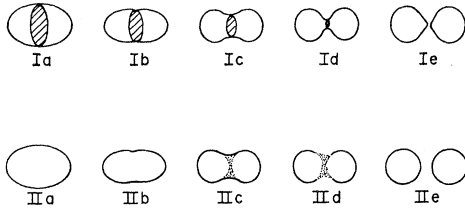


FIG. 1. A schematic description of two different modes of fission. In the first (Ia-Ie) a neck is forming, which becomes continuously thinner until it finally snaps. The hatched cross section describes the "scission surface." In the second (IIa-IIe) a region of lower density is forming in the middle of the nucleus, becoming rarer until the nucleus splits.

should any *additional* kinetic energy imparted to the system (that is, to the nucleons) be transformed entirely into *kinetic* energy of the collective coordinates? Moreover, it is entirely conceivable that the potential energy at a given "point" $\{\xi\}$ will depend both on the total energy of the system, and on its past history. The emphasis in this paper is on the quantitative consequences of various choices of level populations, rather than on formulating an approach based on any specific one.

The Hamiltonian H is known to commute with various operators, which generate a set of conserved quantities and describe the symmetry of the system. Thus

$$[H, \mathbf{J}] = 0, \quad [H, T_3] = 0, \quad [H, R] = 0, \quad (19)$$

where \mathbf{J} is the angular momentum vector operator (associated with spherical symmetry), T_3 is the third component of the isotropic-spin vector (charge conservation) and R any spatial reflection¹⁹ (generating, together with \mathbf{J} , improper orthogonal space transformation). The one-body Hamiltonian h does not necessarily possess all these symmetries. We have purposefully abandoned the spherical symmetry to arrive at shapes which are typical of paths leading to fission. In the same manner we may abandon others. We also recall that the extremum problem will often call for symmetry-lacking solutions because of the special nature (determinantal) of the sought wave functions. Let us consider the case (which is applicable here, but may be easily generalized) in which we have

$$[h, L_z] = 0, \quad [h, T_3] = 0, \quad [h, R_z] = 0. \quad (20)$$

We have chosen z as a preferred symmetry axis. At each "point" $\{\xi\}$ the eigenstates of h are labeled by m , τ_3 , and γ_z corresponding to these operators, and as we assume that they form a complete set, we always have different energies associated with levels having the same set of quantum numbers.

At the same time, levels having different sets of quantum numbers may have the *same* energy. All the

solutions ϕ of the variational problem satisfy

$$\langle \phi_\mu^\sigma | H | \phi \rangle = 0, \quad (21)$$

where ϕ_μ^σ is any state which differs from ϕ by *one* particle. This reflects the relative stability of each of the configurations against excitations of particles by the total Hamiltonian H . Thus there is an increased tendency to conserve the individual quantum numbers of each of the particles. If we consider a subspace in which axial symmetry always holds, we arrive at an alternative rule of population whereby the magnetic quantum number m is individually conserved. A similar consideration holds for the reflection symmetry.

The question now arises as to what happens when any of these symmetries are relaxed. An energy degeneracy which may have existed between states belonging to *different* γ_z is removed once γ_z ceases to be a good quantum number, because of the interaction now operative between the states. The transition between these two states, which the strict conservation of the relevant quantum number would require, must be understood in the following sense. As we have mentioned above, the freedom associated with the particle coordinates is manifested in the multiplicity of solutions to the variational problem. Each such solution, $\phi^i(\{\xi\})$ is an eigenstate of a *different* Hartree-Fock Hamiltonian $h^i(\{\xi\})$. We have simulated, for reasons of simplicity, each $\phi^i(\{\xi\})$ associated with $h^i(\{\xi\})$ by a different solution of the *same*, standardized $h(\{\xi\})$. Thus, two solutions ϕ^i and ϕ^j which viewed in this simulated manner are very similar (different, say, in *one* particle) may have been in fact quite different originally. Also, the energy degeneracy which may exist (and seems to be removed) between two individual *single-particle states* of $h(\{\xi\})$ actually represents a *true* energy degeneracy of the two complete configurations ϕ^i and ϕ^j . We, therefore, may be justified in considering the conservation of individual quantum numbers in this framework.

In practice, the effects of the internal degrees of freedom which are absent in the LDM, may be taken into account in two ways: (i) Explicitly, by actually including the additional coordinates in the calculation to a larger or smaller extent, (ii) implicitly; working in the LDM space, but modifying the LDM potential by adding a *complex, nonlocal, energy-dependent* potential.

These special aspects, which are of a more dynamic character will be discussed elsewhere.

III. PARTICLE LOCALIZATION IN FISSION PROCESS

We have already emphasized the conceptual difference between the LDM and the Independent Particle Model (IPM) in the description of fission. This may be summarized by the difference in the characteristic mean free path of nucleons in nuclear matter; it is very short in the LDM and very long in the IPM.

¹⁹ Giving rise to the *gerade* or *ungerade* nature of states of Ref. 8.

An individual nucleon—in a properly antisymmetrized framework—is described by a highly localized wave function in the LDM, as against a wave function extending over all the nuclear region in the IPM. If we were to construct a rigorous, complete description of the system, the choice of a basis of single-particle wave functions (localized versus extended) would not matter much. However, in an *approximate* theory, the choice of representation may matter a great deal.

We have indicated in anticipation that under certain assumptions, the *potential* energy associated with any nuclear shape (specifically also the nuclear energy) is practically identical in both models. This does not mean that the predictions of both will be identical, since an essential portion of the dynamic information is inherent in the kinetic-energy operator (or in the mass parameters) which, given the potential, is yet to be determined. In this section we pursue a line of investigation which is indirectly related to this specific problem.

Let us consider a generalized, multidimensional space \mathcal{S} , each point s of which may be characterized by a set of generalized coordinates, such as the $\{\xi\}$ discussed above. \mathcal{S} is the modified configuration space in which the fissioning system is described. Each point s of it represents (in the LDM) some nuclear shape. On the other hand, in the IPM each point characterizes an average instantaneous potential in which the independent nucleons move. It is assumed that some basic assumptions about the nature of the motion, such as the incompressibility of nuclear matter, are already incorporated in this description. The first basic difference between the LDM and the IPM in this connection is that for the IPM we must be explicitly aware of the additional degrees of freedom which characterize the actual *occupation* of single-particle states in the potential of the generalized point s , $V(s)$. As we have stated already, forcing the nucleons to occupy the *lowest* orbits, brings about an almost perfect equivalence between the IPM and the LDM *potential* surfaces.

We may now divide \mathcal{S} into two types of points s : $\mathcal{S}^{[1]}$ which represents all simply connected shapes, and $\mathcal{S}^{[2]}$ which represents all *divided* shapes. In other words, shapes characteristic of *prefission* and of *postfission* configurations, respectively. If the ground state, or any initial nuclear state, is represented by a point s_i , $s_i \in \mathcal{S}^{[1]}$, then the fission process is classically described by a path which asymptotically leads to some point s_f , where $s_f \in \mathcal{S}^{[2]}$. To further the classical analog we now specifically consider such a path. Given any spatial shape described by a point s on this path, we draw an imaginary surface σ dividing this shape into two subshapes. In a hydrodynamical flow, (such motion as would be described by a classical LDM) it is possible to trace the evolution of the surface σ along the path the physical system is following. In particular, if the area of σ vanishes in the fission limit, we would

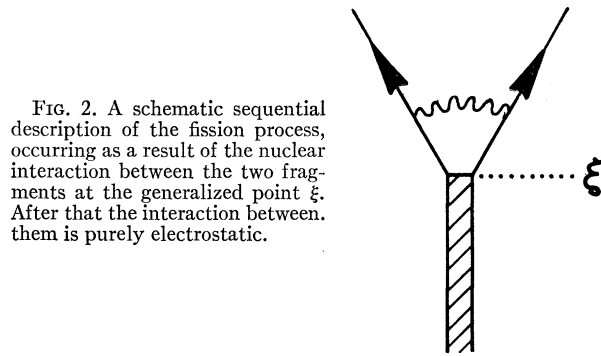


FIG. 2. A schematic sequential description of the fission process, occurring as a result of the nuclear interaction between the two fragments at the generalized point ξ . After that the interaction between them is purely electrostatic.

refer to it as a *scission surface*. It is obvious that along such a classical path, the area of the scission surface varies continuously until it becomes zero. In fact, within the framework of the LDM, this is the only type of sequential process through which fission can occur. The *area* of σ is a direct measure of the interaction (other than electrostatic) existing between the two parts of the fissioning nucleus. Were this interaction switched off, the potential energy of the system would be raised precisely by the amount

$$\Delta E_{\text{pot}} = 2C_{\text{sur}}A_{\sigma}, \quad (22)$$

where A_{σ} is the area of σ . If, for example, the system has enough kinetic energy at this configuration, then such a transition, (from one nucleus to two nuclei “touching” but not interacting) is energetically realizable. In principle, it might also be consistent with the equations of motion, if one takes into account the additional degrees of freedom which are suppressed (or “hidden”) in the LDM treatment. In particular, if one allows variations in the liquid drop local density, one may construct such physical paths which are not characteristic of the LDM. This is illustrated in Fig. 1. Each point s along the path discussed above represents, in the LDM framework, a potential $h(s)$, whose eigenstates are occupied by the independent nucleons. A scission surface separates the potential region into two parts which we shall refer to as $R_R(s)$ and $R_L(s)$ (for right and left). Each single-particle wave function may, therefore, be described by a *pair* of wave functions,

$$\chi = (\chi_L, \chi_R), \quad (23)$$

where χ_L is defined over R_L , and χ_R over R_R only. Employing this separation into left and right, we may also write the single-body Hamiltonian h as a 2×2 matrix operator

$$h \equiv \begin{pmatrix} h_{LL} & h_{LR} \\ h_{RL} & h_{RR} \end{pmatrix}, \quad (24)$$

where the meaning of the various pieces is obvious. In the fission limit, when the left and right regions become totally disconnected, we clearly have

$$h_{LR} = h_{RL} = 0 \quad (25)$$

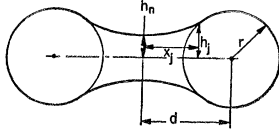


FIG. 3. The type of shapes used in the present calculations, and the parameters (except for α) used to characterize them. The parameters are not independent, since an over-all normalization of volume (or of central density) must be performed.

and the operator h becomes a direct product

$$h = h_{LL} \times h_{RR}.$$

The eigenstates χ of h (in this limit) have the form $(\chi_L, 0)$ or $(0, \chi_R)$. Namely, they are completely *localized* in one of the separated regions, and they belong to the eigenvalues $\{e_L^\alpha\}$ and $\{e_R^\beta\}$ of h_{LL} and h_{RR} , respectively. The only case where an eigenstate of $h_{LL} \times h_{RR}$ may be different from zero in *both* regions, is when some eigenvalue e_L^α is *accidentally* equal to some e_R^β . In such a case any linear combination of $(\chi_L^\alpha, 0)$ and $(0, \chi_R^\beta)$ will be an eigenstate of h . The physical significance of this localization is simple: It states that each of the nucleons of the mother nucleus will definitely find itself in one of the daughter nuclei. It is further suggestive of the possibility that one may forego the necessity of antisymmetrizing particles in the two separate regions.

For any point s , $s \in \mathbb{S}^{11}$, the nuclear wave function is some antisymmetrized product of nucleonic states of the form

$$\phi(s) = \prod_{\alpha=1}^A (\chi_L^\alpha(s), \chi_R^\alpha(s)), \quad (27)$$

where

$$h(s) (\chi_L^\alpha(s), \chi_R^\alpha(s)) = e^\alpha(s) (\chi_L^\alpha(s), \chi_R^\alpha(s)). \quad (28)$$

We now break each of the (orthonormal) single-particle states into

$$\chi^\alpha(s) \equiv (\chi_L^\alpha(s), \chi_R^\alpha(s)) = (\chi_L^\alpha(s), 0) + (0, \chi_R^\alpha(s)) \quad (29)$$

and substitute it into the expression for $\phi(s)$. $\phi(s)$ can therefore be written as a sum of states of the following form:

$$\phi(s) = \sum_{\nu=0}^A \sum_{\{\alpha_i\}} \prod_{i=1}^{\nu} (\chi_L^{\alpha_i}(s), 0) \prod_{j=\nu+1}^A (0, \chi_R^{\alpha_j}(s)), \quad (30)$$

where the summation over $\{\alpha_i\}$ corresponds to all the divisions of a system of A states into two strange subsystems of ν and $A-\nu$ states, respectively. In principle, therefore, $\phi(s)$ is a superposition of states, each of which has a *different* number of particles localized in each region. The liquid drop picture on the other hand, strictly assigns to each region the number of particles consistent with its volume (assuming constant standard density). The amplitude of

each of the components in the *localized states* expansion of $\phi(s)$ must be determined by taking into account the effect of antisymmetrization, recalling that the $(\chi_L^\alpha(s), 0)$ [and likewise the $(0, \chi_R^\alpha(s))$] are not necessarily normalized or orthogonal to one another. To work with these states we define the "localized overlap matrix" K as follows:

$$K_{\alpha\beta}^{(L)}(s) = \langle (\chi_L^\alpha(s), 0) | (\chi_L^\beta(s), 0) \rangle \\ = \int_{\text{Left}} [\chi^\alpha(s)]^* \chi^\beta(s) d\tau \quad (31)$$

and similarly for $K_{\alpha\beta}^{(R)}(s)$. $K_{\alpha\beta}(s)$ depends both on the shape s and on the way the division into the left and the right regions is made, where we clearly have

$$K_{\alpha\beta}^{(L)}(s) + K_{\alpha\beta}^{(R)}(s) = \delta_{\alpha\beta}. \quad (32)$$

The length of each particular state vector in the expansion of $\phi(s)$ is therefore simply

$$\left| \prod_{i=1}^{\nu} (\chi_L^{\alpha_i}(s), 0) \prod_{j=\nu+1}^A (0, \chi_R^{\alpha_j}(s)) \right| \\ = \det K_{\{\alpha_i; i=1, \dots, \nu\}}^{(L)}(s) \times \det K_{\{\alpha_j; j=\nu+1, \dots, A\}}^{(R)}(s), \quad (33)$$

where K^L is a $\nu \times \nu$ determinant giving the overlap integrals of the ν states localized to the left, and similarly K^R is the $(A-\nu) \times (A-\nu)$ determinant for the states on the right. To sum up, $\phi(s)$ can be represented as a general expansion of the form

$$\phi(s) = \sum_{\nu=0}^A a_\nu \phi_\nu^L(s) \phi_{A-\nu}^R(s), \quad (34)$$

where the $\phi_\nu^L(s)$ is a normalized state describing the component of $\phi(s)$ in which ν particles are localized in the left [and similarly for $\phi_{A-\nu}^R(s)$]. The *average* number of particles in each of the subregions is simply given by the integral over this region of the over-all particle density. If the potential which generates the single-particle state is uniform in space (as we have assumed) then this average is simply given by the volume enclosed in each of the regions. However, the expansion of $\phi(s)$ demonstrates the existence of variations (or fluctuations) around this average. This is precisely the equivalent of a cellular expansion of molecules in a gas. The average number of molecules in a given cell of a larger container is proportional to the volume of the cell; the *fluctuations* around this average are of the order of the square root of the number of molecules. In a liquid, where one deals with 10^{23} molecules (or of the order thereof), the fluctuations amount to one part in 10^{11} or so, and may, therefore, be neglected altogether. Inasmuch as the LDM regards the nucleus as a compact liquid (composed of imaginary, infinitely small subparticles) these fluctuations may be neglected in this case as well. The nucleus, however, contains only a small number of particles, and the fluctuations may reach approximately

fifteen particles. Such fluctuations are not negligible and should be incorporated into the dynamics of the system. Realizing, on the other hand, that one has to consider the effect of antisymmetrization, we see that these fluctuations will, in general, be *reduced* from the square-root limit.

To make the point clear, we consider a potential which is symmetric under reflection, but is composed of two separated, completely independent (and of course identical) regions. These regions are the left and right pieces discussed above. Since this idealized picture is supposed to correspond to *prefission* type of potentials, we shall consider the representation in which the eigenstates are either symmetric (gerade) or antisymmetric (ungerade) under reflection. The n th symmetric and antisymmetric states are simply

$$\chi_n^{(+)} = (\chi_n^L, \chi_n^R), \quad \chi_n^{(-)} = (\chi_n^L, -\chi_n^R), \quad (35)$$

where χ_n^L or χ_n^R are the (identical) n th state in one or the other of the separate potentials. We implicitly assume that n refers to an energy ordering—which is identical in both halves of the potential—and completely specifies the state. We now may associate with each n , an occupation number ρ_n whose value would be 0, 1, or 2 depending on whether the n th level is filled in none, one, or both of the fragments. Alternatively, it tells whether none, or both of the pair of states $\chi_n^{(+)}$, $\chi_n^{(-)}$ are occupied. Each determinantal wave function is characterized by such a set of occupation numbers $\{\rho_n\}$. Clearly, any n for which $\rho_n=2$ will correspond to a pair of particles, one of which is localized on the left and one on the right. Therefore, only the levels for which $\rho_n=1$ need be considered in the expansion of the form (30), to calculate the fluctuation in the number of particles. Let \mathfrak{N}_i be the number of levels with $\rho=i$, the relevant expansion surviving antisymmetrization is clearly

$$\phi(s) = \prod_{j=1}^{\mathfrak{N}_2} (\chi_{\alpha_j}, 0) (0, \chi_{\alpha_j}) \prod_{i=1}^{\mathfrak{N}_1} (\chi_{\alpha_i}, (\pm)\chi_{\alpha_i}). \quad (36)$$

Hence, the relative frequency of a fluctuation of ΔA around the mean is simply given by

$$\rho(\Delta A) = \binom{\mathfrak{N}_1}{\frac{1}{2}\mathfrak{N}_1 - \Delta A} \binom{\mathfrak{N}_1}{\frac{1}{2}\mathfrak{N}_1}^{-1}. \quad (37)$$

Thus, the *width* of the number distribution is simply given by $(\frac{1}{2}\mathfrak{N}_1)^{1/2}$. We may apply this result to some more specific cases of the idealized picture.

(i) As we have noted above the (LDM) potential energy is effectively reproduced by populating all the lowest levels. In this ideal case we have for the occupation numbers

$$\begin{aligned} \rho_n &= 2 & \text{for } n \leq \frac{1}{2}A, \\ \rho_n &= 0 & \text{for } n > \frac{1}{2}A. \end{aligned} \quad (38)$$

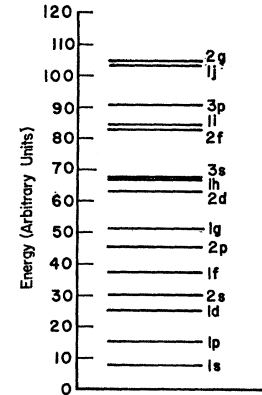


FIG. 4. The energy levels of a spherically symmetric square well of zero depths and infinitely high boundary. The units correspond to $\hbar^2/2M=1$ and to $R=(\frac{2}{3})^{1/3}$.

Thus, $\mathfrak{N}_1=0$ and the width vanishes, as it would in the classical picture of a liquid as well. Therefore, the *assumption of compact level filling* within the IPM, reproduces the LDM also as to the properties of particle localization.

(ii) An alternative way of expressing the occupation described by Eq. (38), is to state that the $\frac{1}{2}A$ lowest-symmetric and $\frac{1}{2}A$ lowest-antisymmetric states are occupied.

We may consider the general case in which the N_+ lowest-symmetric, and the N_- lowest-antisymmetric states are occupied, with N_+ not necessarily equal to N_- . Under this condition we clearly have

$$\mathfrak{N}_1 = |N_+ - N_-| \quad (39)$$

and the width may be quite considerable. If we relax the restriction that the occupied states are the lowest for each reflection symmetry, then we can only write the *inequality*

$$\mathfrak{N}_1 \geq |N_+ - N_-|. \quad (40)$$

(iii) The application of these considerations, coupled with a statistical treatment, may give the behavior of the idealized "localization width" as a function of excitation energy imparted to the system. It is clear that the excitation of the system will generally cause an increase in the average value of \mathfrak{N}_1 . In the limit of infinite energy, we have obviously

$$\mathfrak{N}_1 = A \quad (41)$$

(where A is the total number of particles in the twin systems). This is so because the relative probability of finding two particles at precisely the same state becomes zero when a finite number of particles are distributed in an infinite number of states. In the intermediate-energy region, which for real nuclei for this purpose is of the order of tens of MeV, we may employ a statistical Fermi liquid theory to investigate the behavior of the quantity \mathfrak{N}_1 . This is done in Appendix A. As a rough result we show there that the "localization width" behaves as $E^{3/4}$.

In the case of an arbitrary, *prefission* configuration, the basic features of the discussion above still hold,

TABLE I. A list of the geometrical characteristics of some of the nuclear potentials for which more extensive results are quoted. (The codes assigned to the shapes are arbitrary.) For each of these shapes an asymmetry parameter may be added. Some of these appeared in the course of a dynamic calculation performed elsewhere. Column 6 gives the surface area of each of the equivolume shapes with the volume normalized so that the sphere has a surface area of 4.836.

Shape code	r	d	h_n	h_j	Surface
SPHERE	0.620	(0)	(0.620)	(0.620)	4.836
F1P	0.533	0.213	0.507	0.521	4.988
F2P	0.488	0.390	0.432	0.464	5.264
F6Q	0.460	0.552	0.378	0.427	5.565
F1P6	0.538	0.215	0.457	0.528	5.163
F2S	0.493	0.394	0.394	0.451	5.359
F2S4	0.497	0.397	0.349	0.429	5.480
F6R	0.497	0.398	0.319	0.332	5.541
F8R	0.470	0.564	0.329	0.433	5.698
F8Q2	0.477	0.572	0.286	0.416	5.804
F8Q3	0.481	0.578	0.246	0.365	5.890
F8Q7	0.486	0.583	0.194	0.345	5.979

except that one is forced to make elaborate numerical calculations to arrive at a proper quantitative generalization. The coupling between the two parts is through the common surface, and the energy therein is proportional to this surface area, *independently* of conditions in all other modes of motion. The same is not true for the IPM. To obtain a quantitative measure as well as a qualitative understanding of the coupling through the common field and its dependence on the level occupation, we go back to the overlap matrix K of Eq. (31). K is best expressed in a representation in which h is diagonal and it contains, in principle, the relevant information. We may look at any wave function ϕ and calculate the fluctuation of the Hamiltonian h in it; namely, the quantity

$$\Delta h[\phi] = [\langle \phi | h^2 | \phi \rangle - \langle \phi | h | \phi \rangle^2]^{1/2}, \quad (42)$$

which has the dimension of energy, and can be easily expressed in terms of the eigenenergies of h , and the matrix element of K . If ϕ is an eigenstate of h , then, and only then, the fluctuation $\Delta h[\phi] = 0$. For pre-fission s , and for wave functions describing a number of particles localized in one of the regions, ϕ^L say, $\Delta h[\phi^L]$ is *different* from zero. In fact, Δh may serve as a quantitative measure for the quality of the particular mode of separation described by ϕ^L . In the limiting case described above, the fluctuation of h is zero for *all* localized components of the wave function separately. To obtain a measure for the meaning of the absolute value of Δh in any general case, we investigate the other limit, that of the originally spherically symmetric configuration. The properties of K for this particular case, as well as some of its eigenvalues are summarized in Appendices B and C. Numerical results utilizing such calculations are given in a following section.

The significance of the preceding discussion to the

actual model describing fission is manifold. The existence of fluctuations in the mass number at a given energy and in the energy at a given mass number must be related to the distributions of mass number and energy yield, resulting from a dynamical model of the process. We may describe the dynamics of the process by the following schematic graph (see Fig. 2). The final state describes a particular mode of separating (into mass, charge, energy, etc.) the total nuclear mass, and the initial state is a particular nuclear state. Out of the total Hamiltonian describing the system we single out as a perturbation the interaction (other than electrostatic) between the two regions. The vertex describes the transition (through the switching of this interaction) to two nuclei, and must be considered at all points of configuration space. It is clear from the discussion above, that each mass division, for example, will have significant contributions from points in this space, which ordinarily (namely, in the LDM) would not contribute at all. Moreover, without actually performing a detailed calculation, it is easy to conceive of situations in which the effects of destructive or constructive interference in the calculation of the amplitude will be of major importance. Again, this particular dynamic aspect will be tackled elsewhere.

IV. CALCULATIONS OF MODEL

As the previous section indicated, the basic theoretical, as well as technical problem which we encounter, involves the finding of single-particle wave functions and eigenenergies in wells of arbitrary spatial shapes, of various energy dependence, and with various boundary conditions. This is generalizing and extending the Nilsson work, which essentially gave eigenvalues of an elliptically deformed harmonic oscillator. These deformations and potentials are not generally typical of the fission process. For reasons of compu-

TABLE II. The energy difference (in arbitrary units) between the lowest symmetric and antisymmetric states as a function of m for various reflection symmetric shapes. The difference is an alternate measure of the coupling between the two "halves." In the LDM this direct coupling is simply proportional to h_n^2 which we quote in column 8. It can be seen that the relation between these two measures is not unique.

No.	0	1	2	$\overset{m}{3}$	4	5	h_n^2
SPHERE	7.83	9.80	11.72	13.52	15.30	17.08	
F1P	5.09	5.84	6.35	6.62	6.75	6.72	0.257
F1P6	4.58	4.67	4.43	4.00	3.52	3.06	0.209
F2P	2.96	2.63	2.10	1.56	1.11	0.75	0.187
F2S	2.36	1.57	0.90	0.49	0.26	0.14	0.155
F2S4	1.75	0.84	0.35	0.15	0.07	0.03	0.122
F6R	1.49	0.62	0.23	0.09	0.04	0.01	0.102
F6Q	1.45	0.68	0.24	0.08	0.03	0.01	0.143
F8R	0.66	0.14	0.03	0.005	0.005	0.001	0.108
F8Q2	0.30	0.03	0.004	0.0004	0.0001	0.0002	0.082
F8Q3	0.12	0.01	0.001	0.0001			0.061
F8Q7	0.04	0.002	0.0001				0.038

tational convenience we have restricted the nucleus to shapes which are axially symmetric, but are otherwise completely arbitrary.²⁰ This has the effect of cutting down the number of degrees of freedom to a workable level, without impairing seriously the generality of the considerations and conclusions. The technical aspects of the numerical solution with this assumption are described in Appendix D. Nevertheless, the relaxation of the axial symmetry restriction may have implications which we have already discussed. Before describing in detail the particular calculations reported here, we would like to make the following general remarks. The object of the calculations is *not* to solve quantitative problems related to specific nuclei and their fission. Rather, it is to provide a qualitatively comprehensive and quantitatively meaningful framework which forms an analog, similar system. In that system the essential features of the theory and their relation to experiment are formulated and investigated. This study will thus illustrate what further quantitative treatments should be undertaken, as well as what general statements can be considered as valid for actual physical systems.

The first step that must be taken, is a truncation of the nuclear instantaneous shapes to be considered, over and above the limitation to axially symmetric shapes. Clearly, highly irregular shapes can be excluded. In this paper we consider quantitatively shapes which can be described by a small number of parameters, and which have already been treated in previous studies.²¹ The nucleus is described by two spheres (overlapping

or not), joined by a neck which is a second-order surface of revolution. Figure 3 shows the general type of such shapes. In addition an asymmetry can be introduced for any shape, by means of an additional parameter.

Thus, each shape is described by an axially symmetric surface which is obtained by rotating a line $y(x)$. This line is described by the following parameters: r is the radius of either of the two spheres; d is the separation between the centers of the spheres; h_J is the distance from the symmetry axis of the point where the neck joins the sphere. Alternatively, the coordinate x_J can be specified (see Fig. 3); h_N is the thickness of the "neck at its central point; α is the asymmetry parameter which is introduced for any symmetric shape $y(x)$ by modifying it to $y(x)$ through the following prescription:

$$\begin{aligned}
 |x| > x_J \quad y_\alpha(\alpha x) &= \alpha y(x); \\
 |x| < x_J \quad y_\alpha(\alpha x) &= [1 + (\alpha - 1) |x|/x_J] y(x), && \text{for } x > 0 \\
 |x| > x_J \quad y_\alpha((1/\alpha)x) &= (1/\alpha) y(x); \\
 |x| < x_J \quad y_\alpha((1/\alpha)x) &= [1 + (\alpha - 1) |x|/x_J]^{-1} y(x), && \text{for } x < 0.
 \end{aligned}$$

The ratio of volumes of the two parts is then given approximately by α^6 . The set of parameters (r , d , h_J , h_N , α) defines a shape, which must be normalized through multiplying by an over-all scale factor. The simplest procedure would be to make the volume of the enclosed shape some prefixed constant. It was pointed out by Swiatecki,²² however, that this causes

²⁰ Thus we remove the restriction to second-order surfaces of some previous works.

²¹ I. Kelson, Phys. Rev. **136**, B1667 (1964); J. R. Nix, in *Proceedings of the Third Conference on Reactions Between Complex Nuclei*, edited by A. Ghiorso, R. M. Diamond, and H. E. Conzett (University of California Press, Berkeley, 1963), p. 366.

²² W. J. Swiatecki (private communication). Also Ref. 27, p. 19.

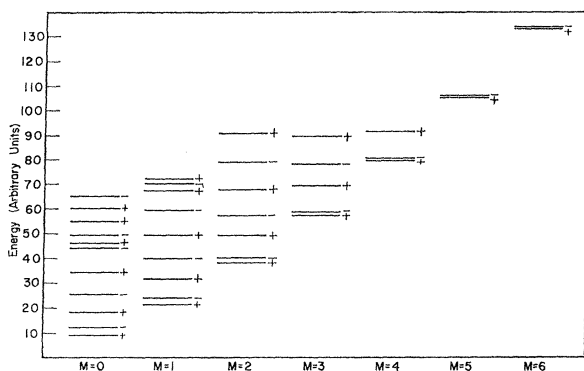


FIG. 5. A typical single-particle energy spectrum for a *symmetric* fissioning potential. The energies are given in the described units, along with m and γ_z of each state. Note the parabolic rise with m of the energy of the lowest m state. The shape is the one coded F2P.

a considerable distortion in the potential energy surface and its derivatives. Rather, one has to normalize the shapes in such a way which reproduces a constant central nuclear density. For a sharp-edged potential well the total single density displays a diffuseness effect near the surface. The falloff of the density to zero on the surface is determined by the wave number of the most energetic nucleons in the system.

As we deal with a prescribed number of particles, there is a constant λ , independent of shape, such that the central density is multiplied by a factor, η , $\eta = [1 + \lambda(\sigma - \sigma_{\text{sphere}})]$, where σ_{sphere} is the surface area of a reference sphere of some given volume V , and σ the surface area for any other shape whose volume is the same. To correct the density back, one has to multiply the volume by η (which is a function of σ). This causes the surface to be modified through multiplication by $\eta^{2/3}$, and the single-particle energies through multiplication by $\eta^{-2/3}$. Thus, if we plot an *unmodified* energy $E(\sigma)$, as a function of σ , we have to modify it through multiplying the abscissa by $\eta(\sigma)^{2/3}$ and the ordinate by $\eta(\sigma)^{-2/3}$. This causes a very substantial modification in the surface energy constant, which becomes $d(\eta^{-2/3}E)/d(\eta^{2/3}\sigma)$ rather than $dE/d\sigma$. However, if we compare *two* curves, $E_1(\sigma)$ and $E_2(\sigma)$, which are not very different from each other, then—since η is a slowly varying function of σ —we have that the *ratio* of surface constants is only slightly changed. Namely,

$$\frac{dE_1}{d\sigma} \bigg/ \frac{dE_2}{d\sigma} \approx \frac{d(\eta^{-2/3}E_1)}{d(\eta^{2/3}\sigma)} \bigg/ \frac{d(\eta^{-2/3}E_2)}{d(\eta^{2/3}\sigma)}.$$

We can, therefore, describe results on such a relative basis, thereby avoiding the central density normalization problem. Surface energy constants would thus be given in terms of a standard LDM surface constant.

The spatial dependence of the potential energy can be chosen in various ways. Since there is no sound physical reason for making any particular choice, we have mostly

worked with a potential which is both natural and technically easy to handle. The potential depth is taken to be *constant*, inside the potential region, and infinite outside. Thus the boundary condition for the single-particle wave functions is the simple requirement that they vanish on the surface. In reality, the surface thickness thus introduced is somewhat smaller than what one would expect on experimental grounds. However, since it is a difference which is independent of the spatial shape, it is hardly of any practical consequence. Similarly, it is possible to modify the behavior of the potential inside the region, but, again, pilot calculations that we have made indicate that this does not add measurably to the understanding of the problem.

An important option in the solution of the single-particle problem is the incorporation of a different boundary condition on the surface, which specifies the value of the *derivative* rather than the value of the wave function on the surface. This is particularly significant for the incorporation of the collective dynamic aspect into the internal, single-particle degrees of freedom.

Thus, for each shape specified by the above parameters, a set of eigenstates are given. Each of these are characterized by the generalized parameters of that particular shape, viz., by m (the z component of orbital angular momentum), by ν (an ordinal number), and, for shapes which possess reflection symmetry through the x - y axis, γ_z (the parity under that operation). The quantum number ν which counts the number of orthogonal states belonging to the same set of other quantum numbers, was limited (for practical reasons) by the relation $\nu < 12$. For actual physical problems, high levels of large m play a very small role, and many were thus not even calculated.

The question of the degree of accuracy in the performance of the numerical calculation is rather intricate. We discuss it, along with examples, in Appendix E.

A particular difficulty is posed by the spin-orbit

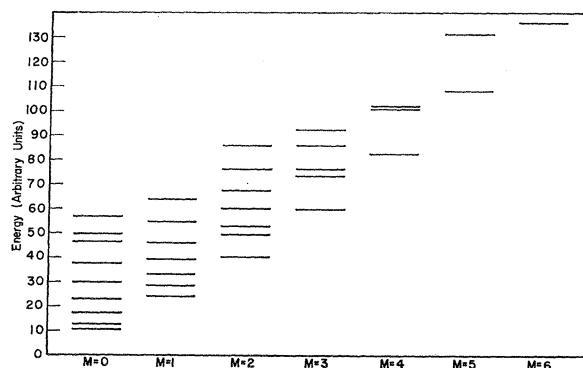


FIG. 6. A typical single-particle energy spectrum for a *non-symmetric* fissioning potential. Note that *increasing* difference between the first two states of each m value.

interaction. For a spherical potential, this operator is well defined and easy to handle. It can be either treated as a perturbation on the purely spatial eigenvalue problem or through modifying this problem into a set of coupled differential equations. When a general shape is treated, the basic definition (and to some extent also the motivation) of a spin-orbit force becomes ambiguous. One can simply adopt the definition which formally extends the spherical case, merely by considering the geometrical center as the origin of the position vector. There is, however, no justification for such a procedure, and, in addition, the passage to two systems, each with its own spin-orbit type internal coupling, becomes rather obscure. Throughout the calculations, however, we have almost exclusively treated the spin-orbit force as a perturbation on the very final state of numerical results, as in Sec. VI.

V. PRESENTATION AND ANALYSIS OF NUMERICAL RESULTS

In this section, we present and analyze results based on the ideas and techniques discussed in the previous sections and in their accompanying appendices. The results are divided into two general categories: (i) those relating to the single-particle field, eigenstates, and eigenfunctions; and (ii) those relating to the multiparticle potential-energy surface and general properties.

We have made an effort throughout the presentation

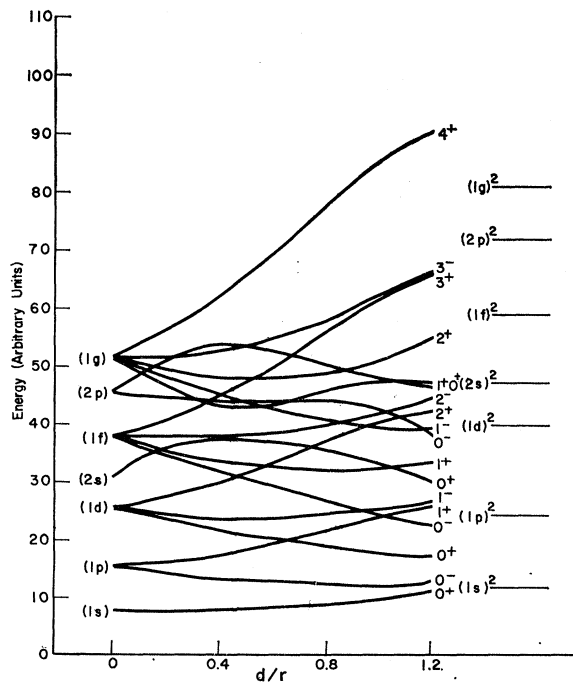


FIG. 7. Variation of single-particle spectrum on an axially symmetric, reflection symmetric fission paths. Shown are the levels corresponding to the spherical $1s$, $1p$, $1d$, $2s$, $1f$, $2p$, $1g$ levels. The asymptotic levels in two separate, identical spheres are shown for comparison on the right.

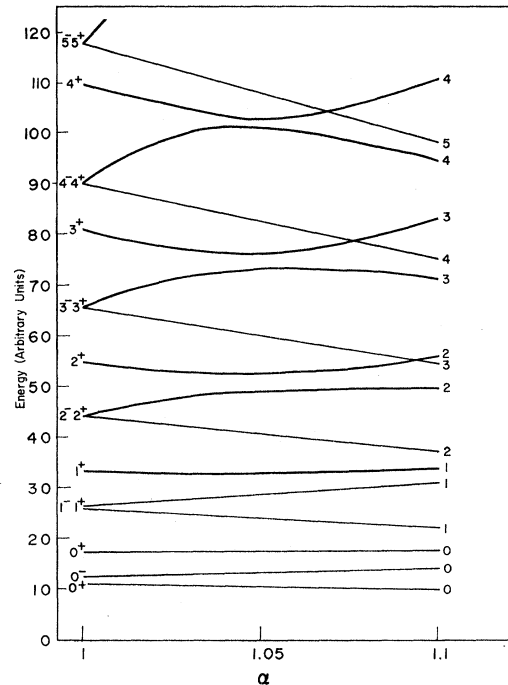


FIG. 8. The variation of the energy levels as a function of α for a particular shape. Only the three lowest levels of each m are shown, to demonstrate their characteristic behavior.

to display results on a *relative* basis, emphasizing the changes due to various modifications without necessarily obtaining their absolute values. Thus, we express most of the pertinent numbers in *arbitrary units*. This is basically made for practical reasons.

In Sec. IV, we have described the parametrized family of shapes (potentials) with which we have been working. As these parameters, five altogether, are not independent, we have essentially a four-parameter family of shapes. In Table I we list the geometrical values of r , d , h_N , h_J of some of the shapes referred to through the text. To each one of them an arbitrary asymmetry parameter α may be assigned. The choice of parameters was mainly dictated by the desire to provide as wide a basis for calculations as possible. Also, some of these particular shapes were encountered in the course of dynamical calculations²¹ (in the LDM framework) and it was felt that their selection might turn out eventually to be useful in a unified dynamical treatment. It must also be emphasized that there is no inherent technical difficulty to bar the evaluation of the properties of particles in an axially symmetric field of arbitrary shape.

From a physical point of view, we may differentiate between distinct types (or modes) of motion. These modes have only an approximate meaning; they are not principal modes in the rigorous mathematical sense, since the kinetic-energy operator is not necessarily diagonal in them. Moreover, they are not generally mutually orthogonal to each other. Nevertheless, we

TABLE III. The probability of localizing in the bigger region of an asymmetric, pinching shape, of the lowest m state. The ratio of the radius of the "neck" to the average radius of the two spheres is also shown for each shape.

$M=$	0	1	2	3	4	5	h_n/r
F1P	0.73	0.82	0.89	0.93	0.95	0.97	0.951
F1P6	0.81	0.89	0.94	0.98	0.99	1.00	0.849
F2P	0.77	0.85	0.91	0.95	0.97	0.98	0.885
F2S	0.86	0.93	0.98	0.99	1.00	1.00	0.799
F2S4	0.91	0.96	0.99	1.00	1.00	1.00	0.702
F6R	0.98	0.99	1.00	1.00	1.00	1.00	0.642
F6Q	0.94	0.98	0.99	1.00	1.00	1.00	0.822
F8R	0.98	0.99	1.00	1.00	1.00	1.00	0.700
F8Q2	0.99	1.00	1.00	1.00	1.00	1.00	0.600
F8Q3	1.00	1.00	1.00	1.00	1.00	1.00	0.511
F8Q7	1.00	1.00	1.00	1.00	1.00	1.00	0.396

find it useful to analyze and discuss the results with specific reference to them. They may be termed as follows: Fissioning mode, essentially governed by changes in d ; pinching (or "necking") mode, changes in h_N ; asymmetrizing mode, changes in α ; fragments internal mode, changes in r and h_J .

The internal fragment mode may call for a larger degree of variety than we have allowed it, as is the case in the work of Nix and Swiatecki.⁹ We also assume that the over-all rotational degrees of freedom have no direct bearing on the *intrinsic* single-particle fields. The initial spherical configuration, and the final two-sphere configurations provide suitable reference points for our discussion. In Fig. 4, we show the eigenvalue spectrum of an infinite square-well of a spherical geometrical form. The eigenstates are labeled by the orbital angular momentum l and by an ordinal (or principal) quantum number n . As is well known, for this case the eigenvalues are immediately derivable from the zeros of the Bessel functions $j_l(x\sqrt{E})$. The overlap matrices K , for a corresponding division into two hemispheres, are given for $m=0$, in Table IV (Appendix B), where their particular structure (as discussed in Appendix C) is readily apparent. The eigenvalues of various submatrices of K , corresponding to various configurations in the spherical potential are shown in Table V. Since the width in the inherent statistical mass distribution is approximately measured by

$$\Delta N \sim \sum e_\lambda(1-e_\lambda), \quad (43)$$

we see that the width is mostly generated (for compact m filling) by the difference between the number of symmetric and antisymmetric states, determining the number of eigenvalues of K which are equal to $\frac{1}{2}$. Clearly, starting with the initial spherical shape in its ground state, we already have this width which is theoretically absent from the LDM. In the other

asymptotic case, all eigenvalues of K are 0, $\frac{1}{2}$ or 1 and we may follow the gradual transition, through fission paths, to this case.

Some typical spectra corresponding to a partially pinched configuration in a symmetric and in an asymmetric case are shown in Figs. 5 and 6. In the symmetric case the levels are also characterized by $\gamma_z(+$ or $-)$ which is the eigenvalue of the reflection operator R_z . One notes that the states of lower m are generally shifted lower than those of higher m , relative to the sphere. This is a characteristic of any prolate deformation, and is also apparent in the Nilsson level scheme. At the same time the density of states of each m varies in a similar manner, namely, the lower the m , the denser the states become.

Since we are dealing with a complicated four-parameter family of shapes, we have a certain degree of arbitrariness in selecting the results to be displayed. In Fig. 7, we show the variation of the independent particle field along a typical path leading to fission with strict reflection symmetry. We note the following features: (i) The lower m levels go down relatively to the higher m levels. (ii) There is a gradual approaching of corresponding levels of opposite R_z symmetry. In the limit of two identical spheres a complete regrouping of levels is carried out. While trend (i) is characteristic of the fission mode, trend (ii) is basically characteristic of the pinching mode (for a symmetric field). In Fig. 8, we show, for a particular shape, the typical dependence of the single-particle spectrum on the asymmetry parameter α . For clarity we show only a few states for each m , where we have also specified their asymptotic reflection symmetry. Figure 8 demonstrates some significant effects. (a) The removal of the reflection symmetry removes the degeneracy between states of the same m , as that which is apparent in Fig. 7. In much the same way, if we were to depart from

the axial symmetry as well, no degeneracy (and hence no level crossing) would occur at any point along this graph. As we have already emphasized, this is a consequence of the *linear* character of the eigenvalue problem. If we believe that each point represents a solution to a *nonlinear* problem (such as the self-consistency problem in fact is) then such degeneracy may in principle occur. (b) The first derivative of the energy $e_{m,\gamma_z,\nu}$ (ν being an ordinal quantum number) at $\alpha=1$ (symmetry) with respect to α , is of great interest. We may, quite generally, express its behavior as follows:

$$\text{sgn}[(\partial e_{m,\gamma_z,\nu}/\partial\alpha)_{\alpha=1}] = -\gamma_z, \quad (44)$$

namely, the symmetric levels tend to go *down* and the antisymmetric levels *up* in energy. If we recall that the asymmetry brings about two nonidentical potential regions, we interpret this observation in a simple way. The symmetric states tend to localize in the *larger* region, and the antisymmetric in the *smaller* region. This is also what one would expect from applying lowest order perturbation theory, since the antisymmetric states are identically zero on the symmetry plane, and the symmetric states are different from zero on that plane. Clearly, once we have moved away from the point $\alpha=1$, this conclusion becomes less and less valid, as the interaction between states of different asymptotic γ_z builds up. (c) We further note the difference in this slope for various values of m . For the lowest ($\nu=1$) symmetric level for each m , the slope is an *increasing function* of m , namely,

$$\Delta/\Delta m [(\partial e_{m,+1,1})/\partial\alpha]_{\alpha=1} > 0. \quad (45)$$

This rule may be coupled with the general observation that the slope is a generally decreasing function (in absolute magnitude) in ν , the ordinal quantum number. The reasons for this behavior are rather simple. The

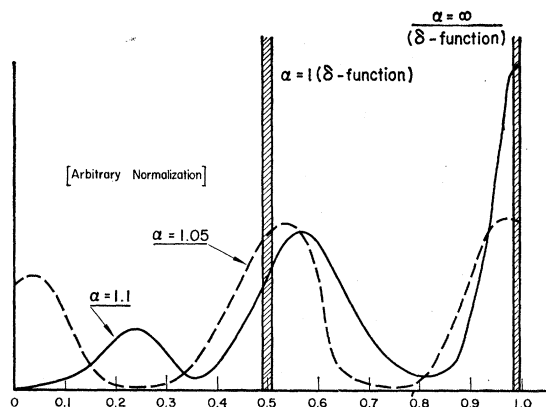


FIG. 9. The distribution of the values of the diagonal matrix elements of the overlap matrix for shape F6Q, for various asymmetry parameters. For $\alpha=1$ the curve corresponds to a δ function, namely, all the diagonal elements are the same, owing to the reflection symmetry. The values $\alpha=1.05$ and $\alpha=1.1$ represent transitions towards the extreme, $\alpha=\infty$.

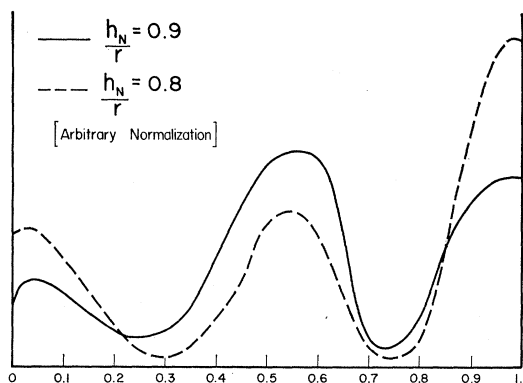


FIG. 10. The distribution of the values of the diagonal matrix elements of the overlap matrix for two asymmetric shapes which differ only in the degree of pinching (measured by the ratio h_N/r). Note the increase in the number of eigenfunctions localized in one region, when the pinching is increased.

higher the ordinal quantum number, the more nodes does the wave function have, and the less likely it is to be influenced by asymmetrizing the shape. Also, the lower m is, the closer to the symmetry axis is the wave function centered, with the same general result. The consequences of this behavior, which are rather basic and general, is to generate a different behavior of the potential-energy surface depending on the level occupation, as we shall see in the second part of the section.

The essential feature which characterized the fission process from all other collective types of motion is the “pinching” mode, which describes the transition to two subsystems with no nuclear interaction between them. The effect on the single particles, is, as we have mentioned before, to cause them to localize in one of the partial regions. One way of observing this effect quantitatively is by looking directly at the single-particle wave functions and calculating the probability that they be in one region. When a degeneracy exists between eigenenergies of the two separate subregions, one may have to form linear combination of the corresponding eigenstates to describe the localized states. Thus, alternatively, one may take the energy difference between these asymptotically degenerate levels as a measure of the localization of these states. An example is given in Table II. The difference is a fast decreasing function of the center cross section as well as of the magnetic quantum number m , although it clearly depends on various other parameters. By looking at the same shapes, but with some asymmetry parameter $\alpha \neq 1$ which removes the degeneracy, we can give the probabilities that the lowest “symmetric” state be in the bigger region (and, almost identically to it, that the lowest “antisymmetric” state be in the smaller one). These are shown in Table III, which demonstrates the extreme localization occurring even at relatively early stages of the pinching. The effect becomes less marked for states with higher ν .

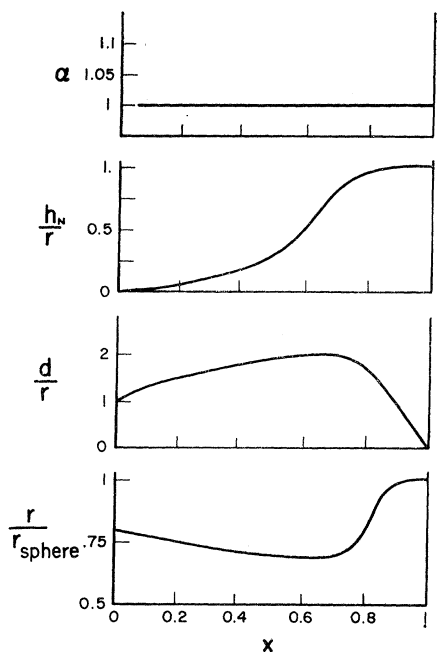


FIG. 11. The dependence of the parameters of the SP shape on the fissionability parameter x . Note the familiar transition one sphere to two touching spheres, as x goes from 1 to 0. The parameters are expressed as the dimensionless ratios α , h_n/r , d/r , and r_{sph} .

In general, the information concerning the interaction between the two subpotentials is inherent in the overlap matrix as well as in the eigenenergies. A direct measure of the individual particle state localization is given by the *diagonal* element of that matrix, although this, as we saw, is not a definitive measure. Some characteristic distributions of these values, for the 200 lowermost states consistent with the magnetic quantum numbers of an initial spherical configuration, are shown in Figs. 9 and 10. In Fig. 9, it is given for a constant shape coupled with various asymmetry parameters. It is easy to see that there is a sizable portion of the particles which appear to be localized predominantly in one part or the other. This portion becomes bigger when the pinching develops, as is apparent from Fig. 10. As a function of the asymmetry parameter, it approaches a δ -function at the value 1, corresponding to the trivial case where the larger part comprises the entire volume. It is interesting to note the concentration around the values 1 and 0.5 (or 0.6), and the great depletion at other values (clearly the average must correspond to the ratio of the volume occupied by the region in question). Some of the characteristics of these curves are spurious, inasmuch as they relate to *exact* eigenstates, instead of correlating different eigenstates belonging to the same quantum numbers and having approximately the same energy. A more consistent way is to observe the *eigenvalues* of the localization matrices. These display the same general characteristics: a gradual passage to a set of δ -function-like spikes situated at 0, 0.5, and 1.0.

It is, incidentally, important to note that the interaction between the two forming fragments is unequally shared by the nucleons. One is essentially reminded of the "nuclear molecular structure",²³ in which clusters are forming inside the dividing nuclear matter, interacting through the exchange of a relatively small number of nucleons at the later stages of fission. Whether or not one can fully expect a "cluster model"²⁴ to work on these grounds is not clear. It is a matter of quantitatively finding whether these clusters are formed (in a statistical sense) before or after the system has evolved through the (classical) saddle-point shape and thus committed to a particular mode of division. As this is a basically dynamic question we shall not attempt here a comprehensive study of it. We shall only conclude by remarking that the cluster model (and also the statistical model²⁵) would generally be expected to improve with lower Z and lower fissionability parameter.

The first task of the LDM is the charting of the potential²⁶ energy surface as a function of the variables $\{\xi\}$ used to describe the physical system. This is the subject of a few studies,⁹ some of which deal with families of curves very similar to the ones dealt with in this paper. In principle, such a chart must be prepared

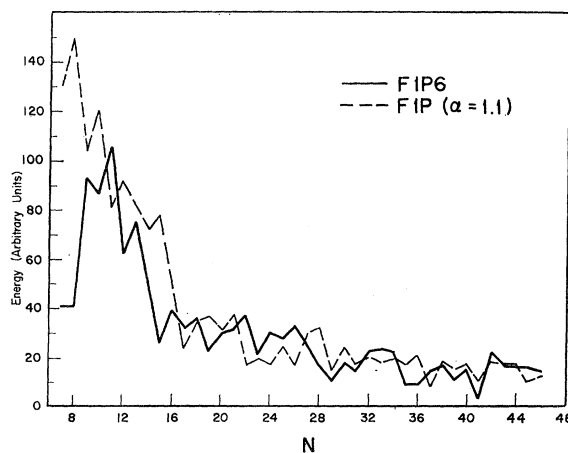


FIG. 12. A display of "direct shell effects" (or dependence on number of particles) for two different shapes, one of which is asymmetric. The ordinate gives (in arbitrary units) the value of

$$\frac{\Delta}{\Delta N} (N^{-5/3} \sum_{i=1}^n e_i),$$

where the spin and isospin degeneracy of the levels is neglected. The solid curve corresponds to shape FIP6; the dashed to FIP ($\alpha=1.1$).

²³ V. M. Strutinskii, N. Ya. Lyashechenko, and N. A. Popov, *Zh. Eksperim i Teor. Fiz.* **43**, 584 (1962) [English transl.: *Soviet Phys.—JETP* **16**, 418 (1963)].

²⁴ H. Faissner and K. Wildermuth, *Nucl. Phys.* **58**, 177 (1964).

²⁵ P. Fong, *Phys. Rev.* **89**, 332 (1953).

²⁶ We wish to emphasize again that the term "potential" is somewhat misleading, as it contains also the kinetic energy of the individual nucleons. It must be understood in the sense of the previous sections.

for every nucleus (Z, A) under consideration. The LDM, however, replaces the potential part of the many-body Hamiltonian by the sum of an electrostatic term

$$V_{\text{els}} = C_c \iint \frac{\rho(\mathbf{r}_1)\rho(\mathbf{r}_2)}{|\mathbf{r}_1 - \mathbf{r}_2|} d^3\mathbf{r}_1 d^3\mathbf{r}_2 \quad (46)$$

and a nuclear surface energy term

$$V_{\text{sur}} = C_s \times (\text{surface area}). \quad (47)$$

This has the effect of smoothing out all the effects which are peculiar to some specific neutron or proton number. It is clear that up to a scaling factor, the potential-energy surface depends only on *one* parameter which measures the relative strengths of V electrostatic and V surface. This fissionability parameter is of basic importance in determining the likelihood of fission for any individual nucleus. It is the electrostatic repulsion which is responsible for the tendency of the nucleus to split, and the nuclear surface cohesion which tries to counteract its effect. The fissionability parameter x is essentially the ratio of the two constants, C_c/C_s , which scale these two forces. When one picks the empirical values of C_c and C_s from fits to data on binding energies of nuclear ground states, one obtains

$$x = Z^2/50.13A^{1/3}. \quad (48)$$

The value $x=1$ represents a nucleus which is already unstable against fission in its spherical ground-state configuration; it provides the actual limit on the stability of nuclides in the upper part of the periodic table.²⁷

Of the various features of the energy surface, perhaps the most interesting is the existence of saddle-point shapes and their properties. Using the terminology of Sec. III, we can define this point as follows: Consider all continuous paths leading from some specific initial configuration s_i , $s_i \in S^{[1]}$ to any point

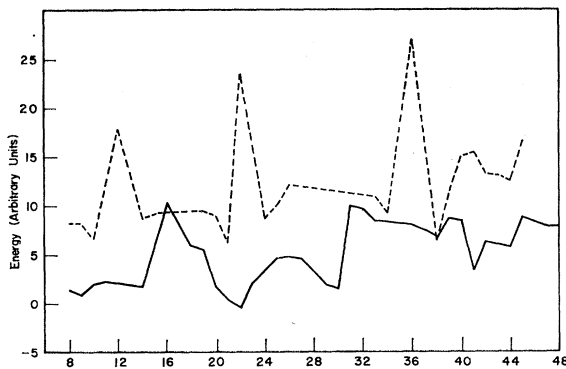


FIG. 13. Two typical cases of "derivative shell effects." The ordinate shows (in arbitrary units) the variation with N of the quantities $\partial V/\partial h_n$ (solid curve) and $\partial V/\partial \alpha$ (dashed curve) for one particular shape F2S.

²⁷ W. Meyers and W. J. Swiatecki, Nucl. Phys. **81**, 1 (1966).

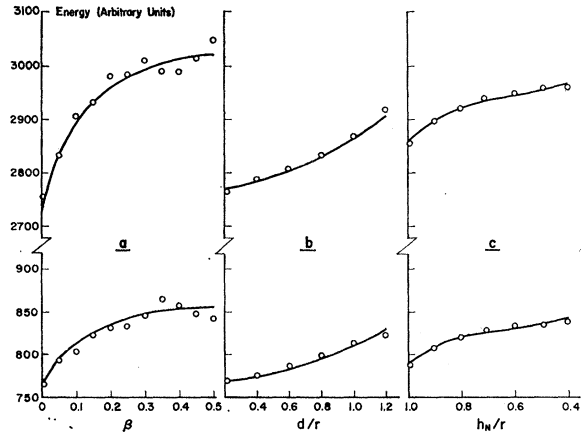


FIG. 14. The total nuclear energy for three types of configurations: (i) two tangent spheres with a varying volume ratio, (ii) a slightly pinched configuration with varying stretching, and (iii) a partly stretched configuration with varying degree of pinching. For each case the graphs for two total number of particles (protons or neutrons)—40 and 92—are given, along with the best fit by a sum of volume and surface-energy terms.

s_f , $s_f \in S^{[2]}$. Since s_i represents a configuration which is locally stable, and the energy at s_f is lower than at s_i , the potential energy attains some maximum value on each of these paths. The lowest of these maxima is then defined as the saddle-point shape, and its height relative to s_i , as the LDM fission barrier. It represents the configuration through which the system is classically most likely to proceed to fission. Mathematically, when we consider the energy surface $V(\xi)$, one demands: (i) For the saddle point ξ_{SP}

$$(\partial V/\partial \xi_i)_{\xi_{\text{SP}}} = 0, \quad i = 1, \dots, n \quad (49)$$

and (ii) all eigenvalues of the second-order derivative matrix $D^{(2)}(\xi_{\text{SP}})$, where

$$D_{ij}^{(2)} = \partial^2 V/\partial \xi_i \partial \xi_j \quad (50)$$

are positive, except for one which is negative. Clearly, if the topology of $V(\xi)$ is complicated, one may encounter many saddle-point shapes satisfying conditions (i) and (ii), as well as other extremum points satisfying (i) but not (ii). If an abundance of SP's occur, one has to fall back on the requirement that the fission barrier is smallest for the proper SP. The actual calculation and finding of the SP shape is rather tedious, basically because of the high accuracy necessary in the performance of the calculation of the six-dimensional electrostatic-energy term for each shape.²⁸ Clearly, also, the SP shape will depend on the nature of the coordinates ξ and their symmetry properties. Nevertheless, enough is known about the behavior of the LDM SP shape as a function of the fissionability parameter from previous studies²¹ and from general considerations. The characteristics of the classical

²⁸ R. Beringer, Phys. Rev. **131**, 1402 (1963).

LDM SP shapes in the framework of this paper are given in Fig. 11. They may be summarized as follows:

- (a) The smaller x , the more removed from the initial configuration the SP shape is.
- (b). The smaller the x , the more pinched the SP shapes and the less matter is concentrated in the "neck."
- (c). For *all* x , the SP shape possesses reflection symmetry through the x - y central plane.

These features are rather general, they are apparent from the curves in Fig. 11, and are quite independent of the rather large numerical uncertainties inherent in the calculation of the absolute magnitude of their values. Property (c) is most striking of all, inasmuch as it confronts the LDM with the challenge of explaining the experimentally observed mass asymmetry in the fission yield distribution.²⁹

The various aspects of the explicit inclusion of the independent particles degrees of freedom will be treated with reference to the classic LDM results. They are essentially described as modifications and additions to them. Furthermore, they are performed and analyzed in such a way, as to make them rather insensitive to the calculational uncertainties of the former. This is done primarily by employing perturbation techniques in the calculation of the SP's as follows: Expand the potential energy $V(\xi)$ around the SP ξ_{SP} :

$$V(\xi) = V(\xi_{\text{SP}}) + \frac{1}{2}(\xi - \xi_{\text{SP}})D^{(2)}(\xi_{\text{SP}})(\xi - \xi_{\text{SP}})^T, \quad (51)$$

where $D^{(2)}$ is the second-order derivative matrix of Eq. (50), and ξ stands for $(\xi_1, \xi_2, \dots, \xi_n)$. We now expand around ξ_{SP} a small perturbation $\bar{V}(\xi)$

$$\bar{V}(\xi) = \bar{V}(\xi_{\text{SP}}) + \bar{D}^{(1)}(\xi_{\text{SP}})(\xi - \xi_{\text{SP}}) + \frac{1}{2}(\xi - \xi_{\text{SP}})\bar{D}^{(2)}(\xi_{\text{SP}})(\xi - \xi_{\text{SP}})^T \quad (52)$$

with $\bar{D}^{(1)}$ standing for the first derivatives column,

$$\bar{D}_i^{(1)} = \partial \bar{V} / \partial \xi_i. \quad (53)$$

Solving the extremum conditions

$$\delta(V + \bar{V}) = 0, \quad (54)$$

we clearly have for the new SP $\bar{\xi}_{\text{SP}}$

$$\bar{\xi}_{\text{SP}} = \xi_{\text{SP}} - [D^{(2)}(\xi_{\text{SP}}) + \bar{D}^{(2)}(\xi_{\text{SP}})]^{-1} \bar{D}^{(1)}(\xi_{\text{SP}}). \quad (55)$$

This procedure is particularly useful for determining the effect of various perturbative terms on the coordinate α which measures the asymmetry of the shape. The most important perturbative terms involve the promotion of particles from occupied to unoccupied nuclear levels.

The results are divided generally into two categories: shell effects and gross properties of the multiple nuclear potential-energy surfaces.

Shell Effects. Under this heading we include all the characteristics of the system which were smoothed off by the LDM potential-energy ansatz, and which reflect dependence on the number of particles. Strictly speaking, shell effects refer to particular discontinuities or irregularities which occur at specific particle numbers. They essentially accompany *any* problem which involves discrete, irregularly spaced eigenvalues. In the spherical shell model, for instance, they are further enhanced by the existence of strong *degeneracies* in the eigenvalue spectrum. As far as the energy of the system is concerned we may distinguish between two general types of shell effects; those which are associated with the *total energy* of the system, and those which are associated with the response of the system to variations and stimuli. The first deals with the function $E(N)$; the second with $\partial E / \partial \xi(N)$. The same two types exist in the nuclear shell model, except that the distinction between them is not always clearly made. The first is responsible for the behavior of binding and separation energies; the second for the behavior of first (and higher) excited states, and of transition probabilities. We should point out that the present calculations indicate empirically that the sphere is the only spatial configuration for which *both types of shell effects occur consistently at the same numbers*. The curves in Figs. 12 and 13 demonstrate the two types of shell effects for various shapes. We may summarize the relevant qualitative characteristics (some of which are displayed in the figures):

(i) Derivative shell effects are much more dramatic than direct shell effects for shapes which possess a lesser degree of symmetry.

(ii) As the shape becomes more pinched, the direct shell effects become dominated by the corresponding effects in the substructures which are being formed. This feature has direct bearing on the validity of application of the cluster and statistical models.

(iii) The shell effects, although very pronounced in many cases, attain varying forms and occur at other nucleon numbers for different shapes. This is significant; it means that although these variations may be sometimes important, and certainly always interesting, we may average them out, indeed, when we investigate characteristics of the system which are independent of the number of particles. In other words, the many-particle nature of the system is preserved throughout the calculation (rather than replacing the Hamiltonian by a "smooth" one), but the variations which are due purely to "shell effects" are subsequently averaged away. One of the major effects which are thus concealed, is the behavior of the fission barrier in the vicinity of closed shell. This basically comes about because the inclusion of the shell structure actually shifts the ground-state configuration away from symmetry. The additional binding energy present for closed shell nuclei causes them generally to be more stable

²⁹ Recall, though, that a symmetric SP does not necessarily imply symmetric division.

against fission than otherwise (with the averaging procedure) might be expected. An exhaustive study of this aspect, for more realistic single-body potentials, was carried out by Nilsson, Swiatecki, and collaborators.

In Figs. 12 and 13, we held the shape of the potential fixed while allowing the number of particles to vary. We now turn our attention to a different presentation, namely, holding the number of particles fixed while changing the shapes of the potentials. This will not only demonstrate characteristics peculiar to the number of particles, but will also help us to try and extract average volume and surface potential-energy terms. This is shown in Figs. 14(a), 14(b), and 14(c). The first of those describes the configuration of two tangent spheres with different radii but with a combined fixed volume. The second and third correspond to more elaborate modes of motion, intermediate in the fission process. For all shapes, two total numbers of particles are quoted, but the figures hold the shapes fixed so that the density normalization is incorporated in the constants necessary to define the volume and surface terms. Figure 14 depicts information which is characteristic of the behavior of the total energy, and show, as we have anticipated, that the IPM becomes essentially equivalent to the LDM when the stipulation

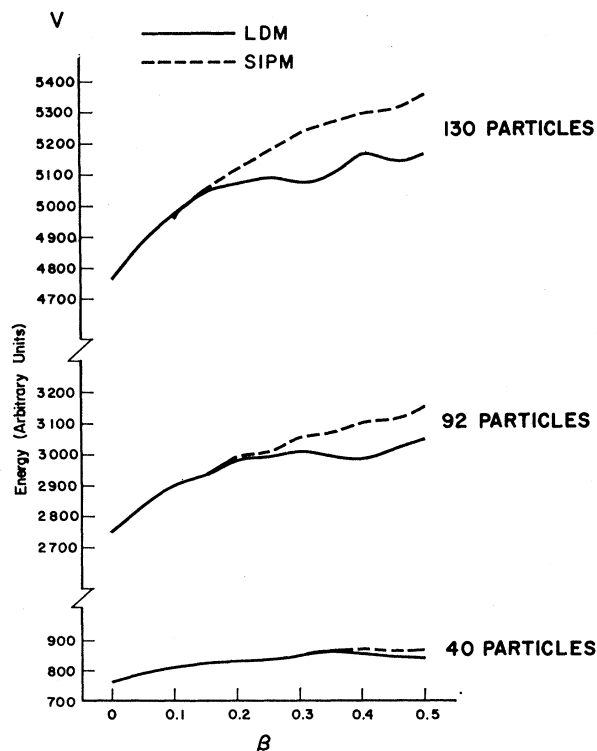


FIG. 15. The variation of $V(\text{LDM}; \beta)$ (solid curves) and $V(\text{SIPM}; \beta)$ (dashed curves) for 40, 92, and 130 particles of a kind, as a function of the fractional mass of one of two tangent spheres. Note the "shell effects" which are quite striking. The shapes are held fixed even though the number of particle varies, and the ordinate is given in arbitrary units.

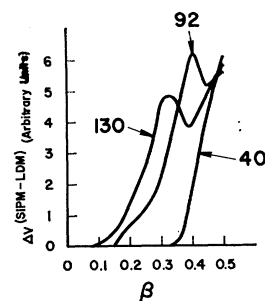


FIG. 16. The difference in arbitrary units between $V(\text{SIPM}; \beta)$ and $V(\text{LDM}; \beta)$ as derived and normalized from Fig. 15.

is made that the nucleons occupy the lowest available orbits. The LDM is thus representative of the gross features of a *special type* of IPM. In general, however, if we just give the generalized coordinates $\{\xi\}$, we would not be specifying the state of system completely. More information which we may symbolically designate by π is necessary, which determines the occupation of single-particle orbits in the potential characterized by $\{\xi\}$. We therefore would have as a function of $\{\xi\}$, not just one potential-energy surface, but an infinite family $V(\pi; \{\xi\})$. The LDM is basically (averaging and neglecting fluctuations) the lower envelope of all surfaces:

$$V(\text{LDM}; \{\xi\}) \equiv \min_{\text{all } \pi} V(\pi; \{\xi\}).$$

It seems intuitively apparent that in any time-dependent description of the system, it will not necessarily be confined to $V(\text{LDM}; \{\xi\})$. Now, although we cannot make any *dynamic* predictions based on the knowledge of all the surfaces $V(\pi; \{\xi\})$ (just as the LDM could not from merely inspecting $V(\text{LDM}; \{\xi\})$), it is nevertheless very instructive to be familiar with their general properties. We begin by noting that a dynamic rearrangement of particles which reproduces the LDM, involves the transition of particles from higher to lower orbits. In particular also, individual quantum numbers may have to be changed in the process. Therefore, we shall look specifically into a limiting case in which individual quantum numbers are *not* altered. Since we are exploring here a model with intrinsic axial symmetry, we shall let the magnetic quantum numbers be the key to the definition of the multiple surfaces $V(\pi; \{\xi\})$. We shall consider configurations in which all magnetic quantum numbers are frozen. The symbol π will then stand for a set of numbers $\{\eta_m\}$, η_m being the number of particles with magnetic quantum number m ; and we further assume that for each m , the η_m occupied levels are the lowest. In an axially symmetric framework this procedure defines an infinite family of mutually nonintersecting potential surfaces $V(\{\eta_m\}; \{\xi\})$, where we clearly have

$$\sum \eta_m = \text{total number of particles.}$$

The potential surface with which we shall be primarily concerned, other than the LDM surface, is

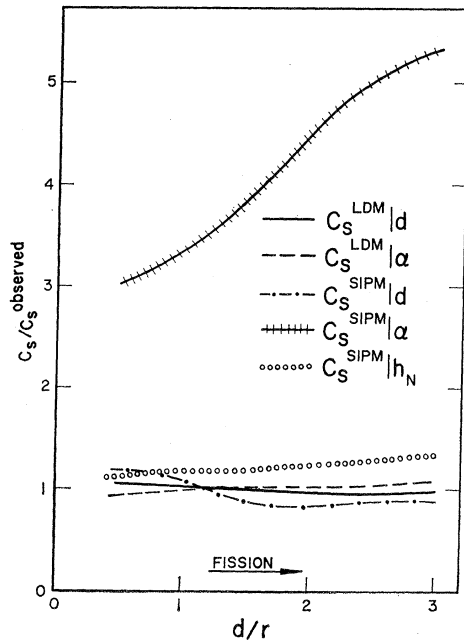


FIG. 17. The extracted quantities $C_S^{\text{LDM}}|_d$, $C_S^{\text{LDM}}|_\alpha$, $C_S^{\text{SIPM}}|_d$, $C_S^{\text{SIPM}}|_\alpha$, $C_S^{\text{SIPM}}|_{h_N}$ as a function of d/r along a typical fission path. The subscripts d , α , h_N refer to the mode for which the surface constant is evaluated. The ordinate unit corresponds to a normalization to the observed surface constant.

that which retains the magnetic quantum numbers of an initial *spherical* configuration; we shall refer to it as SIPM. This is physically significant since the sphere does represent an actual metastable starting point of the fission process. Again we start by looking at the configuration composed of two tangent spheres with a constant combined volume. The abscissa gives the fraction volume in the smaller sphere, with $\beta = \frac{1}{2}$ corresponding to two equal spheres, and $\beta = 0$ to a single sphere. In Fig. 15, a series of curves, for various total particle numbers (again keeping the volume fixed), gives both $V(\text{LDM}; \{\xi\})$ and $V(\text{SIPM}; \{\xi\})$ as a function of the parameter β . Figure 15 displays some important characteristics. As the definition trivially implies, the SIPM values are always larger than or equal to the LDM ones. For each total number of particles A , there is a minimum value $\beta_{\min}(A)$ under which the difference of the two is zero, and over which it monotonically increases with β . This minimum value is itself a monotonically decreasing function of A . Namely, the larger the total number of particles, the more asymmetric is the two-sphere configuration at which the SIPM potential energy begins to differ from the LDM one. This, of course, will also hold for more general configurations. It implies, among other things, that the properties of $V(\text{SIPM}; \{\xi\})$ depend on the total number of particles as well as on the fissionability parameter x . This is in marked contradiction to $V(\text{LDM}; \{\xi\})$. To further demonstrate this point, we extract from Fig. 15 the difference $\Delta V[\text{SIPM-LDM}]$

between the two curves and we normalize all curves through division by a constant proportional to $N^{5/3}$. The results are shown in Fig. 16, where one clearly sees the shell effects superimposed on the general trend of the curves as described above.

We may gain further insight into the properties by considering the electrostatic term in the two tangent sphere configuration as well. We write schematically

$$V(\text{SIPM}; \beta) = [\beta^{2/3} + (1-\beta)^{2/3}] \\ + \hat{x} \left\{ \frac{2}{5} \beta^{5/3} + \frac{2}{5} (1-\beta)^{5/3} + [\beta(1-\beta) / (\beta^{1/2} + (1-\beta)^{1/2})] \right\} \\ + \Delta V[\text{SIPM-LDM}](\beta),$$

where \hat{x} is a constant proportional to the fissionability parameter. For $\hat{x} = 0$ we may replace ΔV by a function which is rigorously monotonic in β , and then the SP of $V(\text{SIPM}; \{\xi\})$ will coincide with that of $V(\text{LDM}; \{\xi\})$, but it will be higher by the amount ΔV at the SP. As \hat{x} becomes larger than zero, the SP becomes truly a saddle point in the sense of the above definitions, and the effect of ΔV which has a nonvanishing derivative at $\beta = 0.5$, is to shift it towards smaller values of β (and asymmetry). Clearly, at the same time the true SP will no longer be on the two-sphere configuration subspace. As β becomes closer to unity, the SP of the LDM potential (exclusive of $\Delta V[\text{SIPM-LDM}]$) approaches the one-sphere configuration. But for this configuration, as we saw, ΔV is negligible, and hence the SP for $V(\text{SIPM}; \{\xi\})$ becomes symmetric once again. The dynamic consequences, however, of the SP symmetry are not quite as clear for $\beta \sim 0.5$ as they are for $\beta \sim 0$, because in the first case the two fragments are hardly defined at the SP configuration.

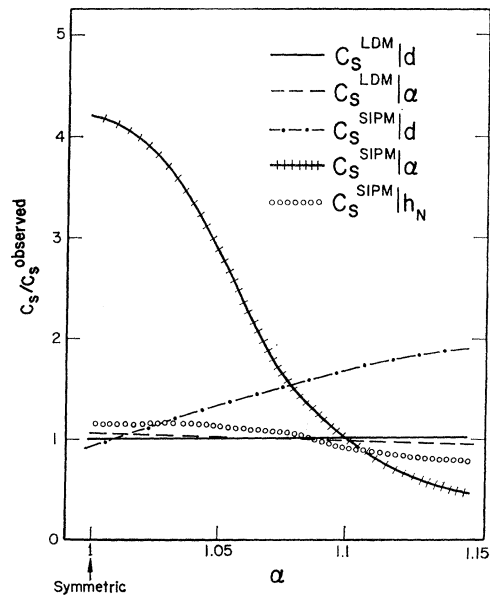


FIG. 18. The extracted quantities $C_S^{\text{LDM}}|_d$, $C_S^{\text{LDM}}|_\alpha$, $C_S^{\text{SIPM}}|_d$, $C_S^{\text{SIPM}}|_\alpha$, $C_S^{\text{SIPM}}|_{h_N}$ as a function of α for a typical semipinched shape.

A detailed mapping of $V(\text{SIPM}; \{\xi\})$ is not presented here for a number of reasons. Firstly, $\{\xi\}$ represents a set of intricately dependent five parameters which make the charting technically unfeasible. Secondly, its properties are basically related through the addition of $\Delta V[\text{SIPM-LDM}]$ to the well-known and widely described LDM potential. Thirdly, $V(\text{SIPM}; \{\xi\})$ is just *one* surface of many [many others being intermediate between $V(\text{SIPM}; \{\xi\})$ and $V(\text{LDM}; \{\xi\})$] and we fear that spending too much effort on its description might overprejudice the reader as to its significance. We find it more useful to extract out of typical cross sections of this surface (and of the LDM one) the surface-energy parameters. These are general functions associated with each of the degrees of freedom $\{\xi\}$, and are defined for any surface through

$$C_s^\pi(\xi) |_{\xi_i} = \left(\frac{\partial V(\pi; \{\xi\})}{\partial \xi_i} \right) \left(\frac{\partial (\text{Surface Area}(\xi))}{\partial \xi_i} \right)^{-1}. \quad (56)$$

Results pertaining to these functions (which are *a priori* not necessarily constant) are schematically presented in Figs. 17 and 18. As we mentioned, these figures clearly demonstrate that there exists a fairly good *constant* C_s^{LDM} which is largely independent of the nuclear shape and of the type of shape variation causing the change in the nuclear surface area. This C_s^{LDM} is naturally identified with the one taken over from the semiempirical mass formula. On the other hand, the SIPM types display a much more elaborate structure of the surface constant, particularly where the asymmetry parameter is involved. The surface constants associated with all modes are of the same order of magnitude as C_s^{LDM} , except for the asymmetrizing mode, for which it is much larger. As is apparent from applying the perturbation on the SP, and as we have already noticed. The transition from the LDM to the SIPM surfaces thus has the basic effect of *shifting the saddle-point shape from symmetry to asymmetry*. At the same time, of course, the other coordinates will change slightly, but this, we feel, is a second-order effect,

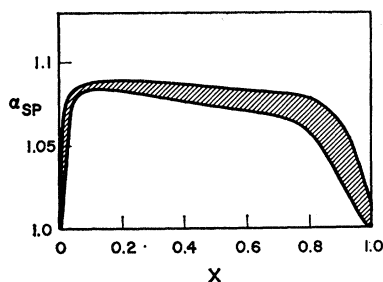


FIG. 19. The variation with x , the fissionability parameter, of the asymmetry parameter α of the SP of the SIPM type surface. The shading represents the uncertainties in the calculation of these values.

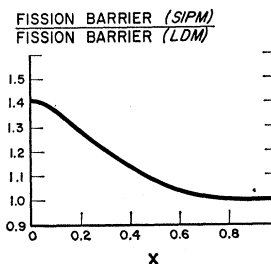


FIG. 20. The ratio of the fission barrier height of the SIPM type surface to that of the LDM type surface. The uncertainties below $x=0.5$ are rather large for other coordinates.

qualitatively as well as quantitatively. In Fig. 19, we plot the dependence of the asymmetry of the SIPM on the fissionability parameter. Were we to insist on the system proceeding through *these* shapes, we would be able to obtain approximate phenomenological rules³⁰ for the mass distribution, as discussed in Sec. VI. It must be remembered though, that in the case of the SIPM there is also the dependence on the *total number* of particles as well as on the fissionability parameters; this dependence has been suppressed in the presentation, and the assumed number of particles (260), roughly agrees with the experimentally interesting ones.

While the SIPM SP shape is asymmetric, the *fission barrier* it predicts is higher than the one predicted by the LDM. In Fig. 20, we plot the *ratio* of the two as a function of the fissionability parameter. It is a rather strong function of x , corresponding to the fact that the lower x , the more particles have to be rearranged to derive the SIPM level occupation from the LDM one. For values near 1, they are identical, because the SP shape is close to the sphere for which the lowest levels and those originally occupied do in fact coincide.

One need not go into detailed dynamic calculations to see the significant implications of these last two figures for the understanding of the mass division in fission, and its dependence on the fissionability parameter. Clearly, the eventual mass division is determined by the relative importance of the SIPM and LDM surfaces. There necessarily is coupling between the two, going through intermediate stages, which will bring about the so-called "slippage" of the system across the surfaces $(\pi; \{\xi\})$. For large fissionability parameters, the SIPM SP shape is close enough to the initial configuration, and its energy is only little higher than the LDM SP, that we may indeed expect it to be dominant in the dynamic process, and to bring about asymmetric fission. As the fissionability parameter goes down, these two arguments become less and less applicable, and we would expect a transition to symmetric fission. This is observed experimentally. Consequently, also, the phenomenological rules which are formulated in Sec. VI are *a priori* expected to hold only for larger values of x , although we have no way at

³⁰ Some heuristic arguments justifying such rules were given in a previous publication: I. Kelson, Phys. Rev. Letters **20**, 867 (1968).

present of predicting where the transition will actually occur.

VI. PHENOMENOLOGICAL RULES

The precise incorporation of the single-particle degrees of freedom into a rigorous dynamic approach is far from simple and is not explicitly tackled in this paper. However, we have proposed,³⁰ some simple rules for the description of the mass-yield distribution as well as for other final distributions resulting from the fission process. It must be emphasized, though, that in the absence of a definitive theory such rules are purely phenomenological and should not be applied indiscriminately.

If we insist on a particular level-filling rule, it is possible to draw conclusions about the behavior of the potential-energy surface. From the discussion in the preceding sections it became obvious that the SP shape associated with various configurations is *not* symmetric, and may thus yield mass divisions which are distinctly unequal. As a simple rule we suggest that the mass ratio of the daughter nuclei be given by A_+/A_- , namely, the ratio of the number of symmetric to antisymmetric (gerade versus ungerade) single-particle states. Since this characterization of single-particle states is rigorously applicable only for potentials (shapes) which possess reflection symmetry, we must understand it in a somewhat modified manner for a general potential. In an asymptotic sense, we may define a "symmetric" state as one which has a crest on the nuclear-scission surface, and an "antisymmetric" state as one which has a node on this surface. The A_+/A_- rule may be visualized in the idealized case described in Appendix D. A configuration of A_+ symmetric and A_- antisymmetric states in a divided potential may be seen as a superposition of limiting cases of various mass divisions. For any specific mass ratio we have an increment in the potential energy for that ratio relative to the LDM potential energy. If the ratio is not unity, we have to adjust the sizes of the two separate potential regions to obtain the actual physical division to which this component corresponds (since the density must be the same in both regions). Under this adjustment, states in the larger piece go down in energy, and in the smaller piece go up. The smallest increment would occur for the case when most of the particles will be in one of the fragments. Hence the ideal preference for the A_+/A_- ratio.

The basic question as far as the A_+/A_- rule is concerned, is in which configuration should this ratio be evaluated. There are two distinct possibilities: (i) the initial ground-state configuration, and (ii) the classical LDM SP configuration. The first possibility was given in a previous publication³⁰ of one of the present authors,

the second was suggested later by Griffin³¹ and seems to be somewhat more consistent with the general picture of the process. Whereas the first (rather than the second) is quantitatively successful for the description of fission of the more fissile (higher Z) elements, it is unsuccessful in accounting for the transition to symmetric fission in the lower Z region. The converse is true for (ii). Inasmuch as we treat this rule at this stage as a purely phenomenological proposition, we present it here without further discussion.

Assuming an initial spherical potential, the nucleonic spatial eigenfunctions are characterized by the quantum numbers n, l, m ,

$$\psi_{nlm} = F_{nl}(r) P_m^l(\cos\vartheta) e^{im\varphi}. \quad (57)$$

Under reflection R_z , $\varphi \rightarrow \varphi$ and $\vartheta \rightarrow -\vartheta$, so that

$$R_z \psi_{nlm} = \gamma_z \psi_{nlm} = (-1)^{l-m} \psi_{nlm}. \quad (58)$$

As l is an integer, there is an *odd* number ($2l+1$) of states in each l multiplet, ($l+1$) having $\gamma_z=1$ and l having $\gamma_z=-1$. Therefore, there are always more symmetric than antisymmetric states, with the difference equal to the number of filled l multiplets in the initial system.

In a deformed initial potential, l is not a good quantum number and the determination of $A_+ - A_-$ (which is supposedly determining the mass difference between the fragments) is not as straightforward. It is easy to see that because of the difference in boundary conditions for symmetric and antisymmetric states on the reflection symmetry plane, ($A_+ - A_-$) is a monotonically increasing function of the nuclear cross section. Hence, the asymmetry in the mass yield distribution in spontaneous fission is a measure of both the sign and the magnitude of the intrinsic nuclear ground-state deformation. Qualitatively we should have for the same hypothetical nucleus

$$(A_+ - A_-)_{\text{oblate}} > (A_+ - A_-)_{\text{spher}} > (A_+ - A_-)_{\text{prolate}}. \quad (59)$$

It is well established that in nuclei there is a strong spin-orbit coupling. The effect of this coupling is to make the half-integer $j (=l+s)$ a good quantum number, along with the half-integer m_j (rather than m and m_s). An eigenstate $|n l j m_j\rangle$ is

$$|n l j m_j\rangle = \begin{bmatrix} l & \frac{1}{2} & j \\ m_j - \frac{1}{2} & \frac{1}{2} & m_j \end{bmatrix} \psi_{nlm_j-1/2} \chi_{1/2} + \begin{bmatrix} l & \frac{1}{2} & j \\ m_j + \frac{1}{2} & -\frac{1}{2} & m_j \end{bmatrix} \psi_{nlm_j+1/2} \chi_{-1/2}, \quad (60)$$

where $\psi_{nlm_j \pm 1/2}$ are the spatial functions of Eq. (57), $\chi_{\pm 1/2}$ spinors, and the bracketed symbols—Clebsch-Gordan coefficients. The states $|n l j m_j\rangle$, therefore, are not invariant under R_z . Rather, they are a combin-

³¹ J. Griffin, University of Maryland Report (unpublished).

ation of states with $\gamma_z=1$ and $\gamma_z=-1$, with probabilities

$$C_{(nljm_j)(\gamma_z)} = \begin{bmatrix} l & \frac{1}{2} & j \\ m_j \mp \frac{1}{2} & \pm \frac{1}{2} & m_j \end{bmatrix}_2$$

for $\gamma_z = (-1)^{l-m_j \pm 1/2}$. (61)

The initial nuclear ground state, inasmuch as it is described as a system of independent particles, is therefore a linear combination of states with different values of A_+ and A_- . The total probability for a certain A_+ (and the complement A_-) is simply

$$P(A_+, A_-) = \sum_{\substack{(\alpha_1 \dots \alpha_{A_+}) \\ (\beta_1 \dots \beta_{A_-})}} \left\{ \prod_{\lambda=1}^{A_+} C_{\alpha_\lambda}^{(+)} \right\} \left\{ \prod_{\mu=1}^{A_-} C_{\beta_\mu}^{(-)} \right\}, \quad (62)$$

where the summation extends over all partitions of the A -nucleon system into an A_+ - and an A_- -nucleon subsystem. Clearly, therefore, the effect of the spin-orbit coupling is to introduce an intrinsic width into the mass distribution. Applying the central limit theorem to this distribution, we rewrite it as

$$P(A_+, A_-) = (2\pi\Gamma)^{-1/2} \exp[-(2\Gamma)^{-1}(A_+ - \langle A_+ \rangle)^2], \quad (63)$$

where

$$\langle A_\pm \rangle = \sum_{\alpha=1}^A C_\alpha^{(\pm)} \quad (64)$$

and

$$\Gamma = \sum_{\alpha=1}^A C_\alpha^{(+)} C_\alpha^{(-)}. \quad (65)$$

For spontaneous fission, the *relative abundance* of a fragment with mass number A_F is proportional to $P(A_F, A-A_F) + P(A-A_F, A_F)$. Normalizing the distribution of A_F to 200%, finally, we have

$$\rho(A_F) = (2\pi\Gamma)^{-1/2} \{ \exp[-(2\Gamma)^{-1}(A_F - \langle A_+ \rangle)^2] + \exp[-(2\Gamma)^{-1}(A_F - \langle A_- \rangle)^2] \}. \quad (66)$$

Figure 21 shows a typical mass yield distribution obtained for the spontaneous fission of Cf^{252} .

The arguments which led to the A_+/A_- rule of thumb apply also to the neutrons and to the protons separately. Thus, the total charge distribution is given by

$$\rho(Z_F) = (2\pi\Gamma_z)^{-1/2} \{ \exp[-(2\Gamma_z)^{-1}(Z_F - \langle Z_+ \rangle)^2] + \exp[-(2\Gamma_z)^{-1}(Z_F - \langle Z_- \rangle)^2] \} \quad (67)$$

with z_\pm and Γ_z analogous to A_\pm and Γ . A similar expression holds for the neutron number. As a rough, general, relation in the limit of a large fissionability parameter we have

$$\langle A_+ \rangle \approx 0.6A, \quad \langle A_- \rangle \approx 0.4A, \quad \Gamma \approx 0.15A \quad (68)$$

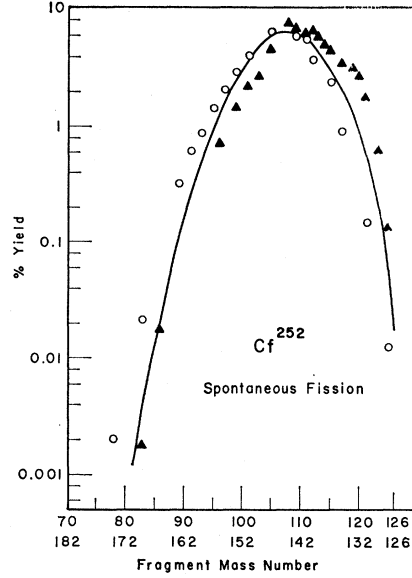


FIG. 21. The theoretical mass-yield distribution for the spontaneous fission of Cf^{252} , and the experimental data (uncorrected for prompt neutron emission). The circles and triangles represent light and heavy fragments, respectively. A prolate deformation with a major to minor axis ratio of 1.4 is assumed.

and similar relations for the corresponding parameters for protons and neutrons.

The distribution of excitation energy of the fragments may also be simply formulated. Assuming the distribution to be directly due to the energy fluctuations in each particular mass and charge division, we immediately obtain a Poisson type distribution. Using a standard energy interval ΔE (to coincide, say, with the average energy necessary for the emission of a neutron) we have

$$P[n\Delta E \leq E_z \leq (n+1)\Delta E] = \exp[-f(Z_F, A_F)] \times [f(Z_F, A_F)]^n / n!. \quad (69)$$

The function $f(Z_F, A_F)$ has to be calculated numerically from the potential-energy surface.

APPENDIX A: CALCULATION OF FLUCTUATIONS IN NUMBER OF PARTICLES AS FUNCTION OF ENERGY

We have twin systems which are given a total excitation energy E . We assume that the excitation energy is large enough to excite a relatively large number of particles, and we treat the systems statistically within the framework of the theory of Fermi liquids. The total excitation energy is distributed between the two liquids according to some probability function $D(E_1, E)$; namely, $D(E_1, E)dE_1$ represents the probability that one of the systems will receive between E_1 and E_1+dE_1 in excitation energy. From the statistical

TABLE IV. The $m=0$ localization overlap matrix, corresponding to the symmetric division of spherical square-well with infinite boundary. The levels are labeled by an ordinal quantum number ν , and by γ_z .

	1 ⁺	2 ⁻	3 ⁺	4 ⁺	5 ⁻	6 ⁻	7 ⁺	8 ⁺	9 ⁻	10 ⁺	11 ⁻
1 ⁺	0.5	0.415	0	0	-0.136	-0.105	0	0	-0.073	0	-0.073
2 ⁻		0.5	0.237	-0.121	0	0	-0.048	0.044	0	-0.019	0
3 ⁺			0.5	0	0.365	-0.047	0	0	-0.135	0	0.054
4 ⁺				0.5	0.093	0.388	0	0	-0.069	0	-0.087
5 ⁻					0.5	0	0.277	-0.056	0	-0.015	0
6 ⁻						0.5	0.024	0.228	0	-0.158	0
7 ⁺							0.5	0	0.348	0	-0.035
8 ⁺								0.5	0.053	0	0.360
9 ⁻									0.5	0.026	0
10 ⁺										0.5	0.119
11 ⁻											0.5

theory we can write the average occupation of a single particle at energy ϵ , as a function of energy $\bar{n}(\epsilon, E)$. The density of single-particle states at this energy is denoted by $\rho(\epsilon)$. The average number of states with occupation number 1, may therefore be simply approximated by the following double integral:

$$\bar{\mathfrak{N}}_1(E) = 2 \int_0^E dE_1 D(E_1, E) \int_{-\infty}^{\infty} d\epsilon \rho(\epsilon) \times \{ \bar{n}(\epsilon, E_1) [1 - \bar{n}(\epsilon, E - E_1)] \}. \quad (\text{A1})$$

Namely, for each possible division of energy, properly weighted, we sum over all single-particle energy states the average probability that one of the levels at this energy is filled while the other is not. The factor 2 stems from the symmetry of the two systems.

To perform the actual calculation we need explicit expressions for the functions $D(E_1, E)$, $\rho(\epsilon)$, and $\bar{n}(\epsilon, E_x)$. For $\rho(\epsilon)$ we take, according to simple phase space argument

$$\rho(\epsilon) = C_1 \sqrt{\epsilon}. \quad (\text{A2})$$

$D(E_1, E)$ is related to the density of states of the whole system at excitation energy E_x , $\hat{\rho}(E_x)$ through

$$D(E_1, E) = \hat{\rho}(E_1) \hat{\rho}(E - E_1) / \int_0^E \hat{\rho}(E_1') \hat{\rho}(E - E_1') dE_1' \quad (\text{A3})$$

for $\hat{\rho}(E_1)$, a few model prescriptions are available,³² and we may choose the functional form:

$$\hat{\rho}(E) = \exp[(C_2 E)^{1/2}]. \quad (\text{A4})$$

Neglecting the chemical potential, setting the Fermi energy at zero, and neglecting any interparticle cor-

relations we write

$$\bar{n}(\epsilon, E_x) = [1 + \exp(E/C_3 E_x)]^{-1}. \quad (\text{A5})$$

The constants C_1 , C_2 , C_3 depend on the systems' dimensions and characteristics, on the units used and to some extent on the models employed here.

At intermediate energies we may deduce the general behavior of $\bar{\mathfrak{N}}_1$ (and hence of the fluctuations in the number of particles) by making some approximations in (A1). Assuming an equal division of excitation energy we reduce the problem to a one-dimensional integral

$$\bar{\mathfrak{N}}_1(E) \propto \int_{-\infty}^{\infty} d\epsilon (\sqrt{\epsilon}) \times \left[\frac{1}{1 + \exp(2\epsilon/C_3 E)} - \frac{1}{[1 + \exp(2\epsilon/C_3 E)]^2} \right]. \quad (\text{A6})$$

Changing the integration variable to $x = 2\epsilon/C_3 E$, we write

$$\bar{\mathfrak{N}}_1(E) \propto E^{3/2} \int_{-\infty}^{\infty} dx (\sqrt{x}) \left[\frac{1}{1 + e^x} - \frac{1}{(1 + e^x)^2} \right]. \quad (\text{A7})$$

Hence, $\bar{\mathfrak{N}}_1(E)$ is approximately proportional to $E^{3/2}$ and the width is proportional to its square root or $E^{3/4}$. The region of validity of the statistical, and other approximation is determined by the requirement that the average number of excited particles will be large, yet small in comparison with the total number of particles. We require, therefore, that

$$\frac{1}{4} A^2 \gg E \rho(0) \gg 1, \quad (\text{A8})$$

where $\rho(0)$ is the density of single-particle states at the Fermi level and $\frac{1}{2} A$ is the total number of particles in each subsystem. Taking as typical numbers $\rho(0) = 5 \text{ MeV}^{-1}$ and $A = 200$, we find that E has to be of the order of 10^1 – 10^2 MeV .

³² J. M. B. Lang and K. J. LeCouteur, Proc. Phys. Soc. (London) A67, 586 (1954).

TABLE V. The eigenvalues of submatrices of the matrix of Table IV, varying the dimension. Note the special structure of the eigenvalues.

Submatrix dimension	Eigenvalues										
1	0.5										
2	0.915	0.085									
3	0.978	0.5	0.022								
4	0.993	0.5	0.5	0.007							
5	0.997	0.895	0.5	0.105	0.003						
6	0.999	0.909	0.889	0.111	0.091	0.001					
7	0.999	0.988	0.899	0.5	0.101	0.012	0.001				
8	0.999	0.989	0.964	0.5	0.5	0.036	0.011	0.001			
9	0.999	0.998	0.965	0.878	0.5	0.122	0.035	0.002	0.001		
10	1.000	0.999	0.990	0.880	0.5	0.5	0.120	0.010	0.001	0.000	
11	1.000	0.999	0.995	0.897	0.876	0.5	0.124	0.103	0.005	0.001	0.000

APPENDIX B: OVERLAP MATRIX K FOR HEMISPHERE

We have mentioned in the text the significance of the overlap matrix K . As a reference case we calculate it here for the particular case of a spherical infinite square-well. Working in the (n, l, m) representation we write, for K defined on a hemisphere

$$K_{nlm,n'l'm'} = \int_{\text{hemi}} \psi_{nlm}^* \psi_{n'l'm'} d\tau. \tag{B1}$$

Using spherical coordinates we put

$$d\tau = r^2 dr \sin\vartheta d\vartheta d\varphi, \tag{B2}$$

$$\psi_{nlm} = f_{nl}(r) P_m^l(\cos\vartheta) e^{im\varphi} \tag{B3}$$

with the integration extending over

$$\begin{aligned} 0 \leq r \leq R, \\ 0 \leq \varphi \leq 2\pi, \\ 0 \leq \vartheta \leq \frac{1}{2}\pi. \end{aligned} \tag{B4}$$

Hence, the integral (B1) separates as follows:

$$\begin{aligned} K_{nlm,n'l'm'} &= \int_0^R f_{nl}^*(r) f_{n'l'}(r) r^2 dr \\ &\times \int_0^{\pi/2} P_m^{l*}(\cos\vartheta) P_{m'}^{l'}(\cos\vartheta) \sin\vartheta d\vartheta \\ &\times \int_0^{2\pi} \exp[i(m-m')\varphi] d\varphi. \end{aligned} \tag{B5}$$

The azimuthal integration over φ yields $2\pi\delta_{mm'}$, and we are left with a product of an angular integral and a radial integral.

The angular ϑ integral, transformed to the coordinate $x = \cos\vartheta$ is simply

$$I_{m,l'}^{(l)} = \int_0^1 P_m^l(x) P_{m'}^{l'}(x) dx. \tag{B6}$$

First we note that the symmetry properties of the associated Legendre polynomials may be utilized as follows:

$$\begin{aligned} \int_{-1}^1 P_m^l(x) P_{m'}^{l'}(x) dx &= \frac{2}{2l+1} \frac{(l+m)!}{(l-m)!} \delta_{ll'} \\ &= \int_{-1}^0 P_m^l(x) P_{m'}^{l'}(x) dx \\ &\quad + \int_0^1 P_m^l(x) P_{m'}^{l'}(x) dx \\ &= \int_0^1 P_m^l(-x) P_{m'}^{l'}(-x) dx \\ &\quad + \int_0^1 P_m^l(x) P_{m'}^{l'}(x) dx \\ &= [1 + (-1)^{l+l'}] \\ &\quad \times \int_0^1 P_m^l(x) P_{m'}^{l'}(x) dx. \end{aligned} \tag{B7}$$

Hence,

$$I_{m,l'}^{(l)} = \frac{1}{2l+1} \frac{(l+m)!}{(l-m)!} \delta_{ll'} \text{ for } (l+l') \text{ even.} \tag{B8}$$

To calculate the general case, we note that $P_m^l(x)$ can be expressed as a polynomial in x , $Q_m^l(x)$ multiplied by $P_m^m(x)$:

$$P_m^l(x) = P_m^m(x) \sum_{\alpha} q_{m,\alpha}^l x^\alpha, \tag{B9}$$

where the coefficients $q_{m,\alpha}^l$ satisfy the differences equation

$$(l-m)q_{m,\alpha}^l + (l+m-1)q_{m,\alpha}^{l-2} - (2l-1)q_{m,\alpha-1}^{l-1} = 0 \quad (\text{B10})$$

with

$$q_{m,\alpha}^l = 0 \quad \text{for } \alpha < 0; \alpha > l-m; \quad l < m \quad (\text{B11})$$

and

$$q_{m,0}^m = 1. \quad (\text{B12})$$

Therefore we have to calculate integrals of the form

$$T_{m\lambda} \equiv \int_0^1 x^\lambda [P_m^m(x)]^2 dx. \quad (\text{B13})$$

Substituting

$$P_m^m(x) = (2m-1)!!(1-x^2)^{m/2}. \quad (\text{B14})$$

We have

$$T_{m\lambda} = [(2m-1)!!]^2 \int_0^1 x^\lambda (1-x^2)^m dx \\ = \frac{[(2m-1)!!]^2 (2m)!! (\lambda-1)!!}{(2m+\lambda+1)!!} \quad (\text{B15})$$

and

$$I_{m,l\nu}^{(\theta)} = \sum_{\alpha,\beta} q_{m,\alpha}^l q_{m,\beta}^{\nu} T_{m(\alpha+\beta)}. \quad (\text{B16})$$

Radial integral. The radial functions in a square-well are given by

$$f_{nl}(r) = r^{-1/2} J_{l+1/2}(k_n r), \quad (\text{B17})$$

where k_n is the wave number such that $J_{l+1/2}(k_n R) = 0$. For $l=l'$ we may use the following relation:

$$I_{nl,n'l'}^{(r)} = \int_0^R r J_{l+1/2}(k_n r) J_{l'+1/2}(k_n r) dr \\ = \frac{k_n r J_{l+1/2}(k_n r) J_{l-1/2}(k_n r) - k_n r J_{l-1/2}(k_n r) J_{l+1/2}(k_n r)}{k_n^2 - k_n'^2} \Big|_0^R \\ = -\frac{1}{2} R^2 J_{l-1/2}(k_n R) J_{l+3/2}(k_n R) \delta_{nn'}. \quad (\text{B18})$$

For the general case, $l \neq l'$ we utilize the explicit expansion of the Bessel function

$$J_p(x) = \sum_{\lambda=0}^{\infty} (-1)^\lambda \frac{x^{p+2\lambda}}{2^{p+2\lambda} \lambda! \Gamma(p+\lambda+1)} \quad (\text{B19})$$

and we get

$$I_{nl,n'l'}^{(r)} = R^2 \sum_{\alpha=0; \beta=0}^{\infty} \frac{(-1)^{\alpha+\beta} (\frac{1}{2} k_n R)^{l+1/2+2\alpha} (\frac{1}{2} k_n' R)^{l'+1/2+2\beta}}{(l+l'+3+2\alpha+2\beta) \alpha! \beta! \Gamma(l+\frac{3}{2}+\alpha) \Gamma(l'+\frac{3}{2}+\beta)}. \quad (\text{B20})$$

This expansion converges very fast. The results of this calculation are summarized in Tables IV and V.

APPENDIX C: SOME PROPERTIES OF OVERLAP MATRICES

(i) Let the Hamiltonian h commute with some one-body operator Ω , then ω the eigenvalues of Ω may be used to label the eigenstates of h , and hence the representation in which K is written. If, furthermore, h_{LL} commutes with Ω (and consequently also h_{RR}), then K is diagonal in ω . For example, if h describes an axially symmetric field and the division into "left" and "right" leaves both regions axially symmetric, K will break into a sequence of submatrices each characterized by a magnetic quantum number m .

(ii) Let the Hamiltonian h be symmetric under reflection, and hence its eigenstates are either symmetric or antisymmetric under reflection (and shall be designated by s_α and a_β , respectively). Let the division into "left" and "right" be made through the symmetry plane. We clearly have

$$K_{s_\alpha s_\beta}^{(L)} = K_{s_\alpha s_\beta}^{(R)}, \quad (\text{C1})$$

$$K_{a_\alpha a_\beta}^{(L)} = K_{a_\alpha a_\beta}^{(R)}. \quad (\text{C2})$$

From the general orthonormalization requirement

$$K_{\alpha\beta}^{(L)} + K_{\alpha\beta}^{(R)} = \delta_{\alpha\beta}, \quad (\text{C3})$$

it therefore follows

$$K_{s_\alpha s_\beta}^{(L)} = K_{a_\alpha a_\beta}^{(L)} = \frac{1}{2} \delta_{\alpha\beta} \quad (\text{C4})$$

and the only matrix elements (other than the diagonal) are those which connect states of opposite symmetry. The matrix $(K^{(L)} - \frac{1}{2})$ has thus the property that, there are two groups of states such that matrix elements between states belonging to the *same* group vanish. Let the number of states in each group be N_+ and N_- , with $N_+ \geq N_-$. We shall now show that for such matrices: (a) At least $(N_+ - N_-)$ of the roots are zero. (b) If λ is a root, so is $-\lambda$; namely, the roots come in pairs with opposite signs. To prove these properties we note that the determinant of any such matrix vanishes if $N_+ \neq N_-$. We now expand the characteristic polynomial of K in terms of the central minors

$$P(x) = \sum_{n=0}^{N_++N_-} (-x)^{N_++N--n} D_n, \quad (\text{C5})$$

TABLE VII. The calculated and the exact single-particle eigenvalues in a sphere. The 11 lowest eigenvalues are given in the column $E(nl)$, while the calculated magnetic components (which should all be the same) are listed under their respective quantum number m .

nl	$E(nl)$	$M=0$	$M=1$	$M=2$	$M=3$	$M=4$	$M=5$
1s	7.532	7.533					
1p	15.406	15.410	15.408				
1d	25.345	25.339	25.339	25.330			
2s	30.126	30.137					
1f	37.266	37.289	37.286	37.290	37.284		
2p	45.541	45.558	45.562				
1g	51.101	51.175	51.153	51.144	51.131	51.120	
2d	63.126	63.085	63.085	63.099			
1h	66.802	66.756	66.762	66.755	66.789	66.798	66.760
3s	67.791	67.864					
2f	82.812	82.909	82.900	82.888	82.854		

Hence, the coefficients of each of the d_α satisfy

$$0 \leq \sum_{\beta=1}^l |O_{\beta\alpha}|^2 \leq 1 \quad (\text{C14})$$

and the maximum $N_l^{(L)}$ will be attained when the coefficients of the *largest* roots are equal to unity (and hence of the other roots equal to zero). Thus,

$$\max N_l^{(L)} = \sum (l \text{ largest roots of } K). \quad (\text{C15})$$

In the particular case discussed above (N_+ symmetric and N_- antisymmetric states), ($N_+ - N_-$) of the eigenvalues of K are exactly equal to $\frac{1}{2}$, N_- are larger than $\frac{1}{2}$ and N_+ are smaller than $\frac{1}{2}$. Thus, for $l \leq N_-$ it is possible to achieve large maximum densities; for $N_- \leq l \leq N_+$ the maximum average densities vary in a standard fashion, and for $l \geq N_+$ they are modified further only slightly.

APPENDIX D: METHODS OF SOLUTION

The basic single-particle equation, in its general form, reads

$$\{-\hbar^2/2M \nabla^2 + V\} \psi = E\psi, \quad (\text{D1})$$

where M is the particle mass, ∇^2 the Laplacian operator, and V the potential in which the particle moves. We shall choose the units such, that $\hbar^2/2M = 1$.

We shall first consider the eigenenergies E , and eigenfunctions ψ , of a restricted case of Eq. (D1). The potential V is taken to be infinite outside a given axially symmetric region and is finite and possesses axial symmetry inside it. Actually, only the axial symmetry is necessary to render the problem feasible. We demand that ψ shall be well defined and integrable.

The problem is suitable for treatment in cylindrical coordinates r, z, φ , where the z axis is the axis of sym-

metry. Transforming Eq. (D1) into cylindrical coordinates, one obtains

$$\left\{ -\left[\frac{1}{r} \frac{\partial}{\partial r} \left(r \frac{\partial}{\partial r} \right) + \frac{\partial^2}{\partial z^2} + \frac{1}{r^2} \frac{\partial^2}{\partial \varphi^2} \right] + V(r, z) \right\} \psi = E\psi. \quad (\text{D2})$$

The boundary condition on ψ is

$$\psi(R_0(z), z, \varphi) = 0, \quad (\text{D3})$$

where $r = R_0(z)$ is the curve in the (r, z) plane, whose rotation around the z axis defines the region in which V is finite. Outside this region ψ vanishes.

We now make the usual ansatz

$$\psi(r, z, \varphi) = r^{-1/2} U_m(r, z) \exp(im\varphi) \quad (\text{D4})$$

obtaining the following eigenvalue equation for $U_m(r, z)$:

$$\{-\left[(\partial^2/\partial r^2) + (\partial^2/\partial z^2) + (\frac{1}{4} - m^2)/r^2 \right] + V(r, z) - E\} U_m(r, z) = 0. \quad (\text{D5})$$

m is an integer and is the z component of orbital angular momentum, characterizing each individual eigenstate. This characterization is a direct consequence of the axial symmetry in the problem. As is known, m determines the asymptotic behavior of $U_m(r, z)$ for small r ,

$$U_m(r, z) = r^{m+1/2} \sum_{\nu=0}^{\infty} A_m(z) r^{\nu}. \quad (\text{D6})$$

To treat the problem numerically, we replace the differential equation (D5) by a set of difference equations. We cover the finite domain, in which U does not vanish, by a rectangular lattice with mesh size $h \times k$, and denote the point $(r = ih; z = jk)$ by (i, j) . The function $U_m(r, z)$ is approximated by a discrete

function $P_{i,j}$, which is defined for all the lattice points inside the potential region. Correspondingly, Eq. (D5) can be written as a finite set of equations

$$\begin{aligned}
 &-(1/h^2)(P_{i+1,j}+P_{i-1,j}-2P_{i,j}) \\
 &-(1/k^2)(P_{i,j+1}+P_{i,j-1}-2P_{i,j}) + (-[(\frac{1}{4}-m^2)/i^2h^2] \\
 &+V(ih,jk)-E)P_{i,j}=0 \quad (D7)
 \end{aligned}$$

with i and j running over the internal points of the region. For points near the boundary $r=R_0(z)$, however, (D7) have to be modified to account for boundary condition (D3). This is done in a standard way.³³ On the axis, we could write the boundary condition $P_{0,j}=0$, which follows from the requirement that $r^{-1/2}U$ is finite there. To determine appropriately the form of the difference equations near the boundary $r=0$, we need investigate the error, introduced by replacing (D5) by (D7). Using Taylor's theorem this error is easily shown to be

$$\begin{aligned}
 E_{i,j} &= (h^2/12)(\partial^4/\partial r^4)U_m(ih+\partial h,jk) \\
 &+ (k^2/12)(\partial^4/\partial z^4)U_m(ih,jk+\partial'k), \quad (D8)
 \end{aligned}$$

where $-1 < \partial$ and $\partial' < 1$. From Eq. (D6) it follows that $\partial^4 U_m/\partial r^4$ behaves as $r^{m-7/2}$ for $r \rightarrow 0$. Thus for $m \leq 3$ the error becomes more and more significant as the symmetry axis is approached, and threatens to impair the accuracy of the calculations. This indeed was found to be the case in actual computations. To overcome this difficulty, we limit the use of Eqs. (D7) to i greater than some i_0 .

The values of $P_{i_0,j}$ will be determined, by imposing the asymptotic behavior (D6). For each j , an additional relation between $P_{i_0,j}$ and $P_{i_0+1,j}, P_{i_0+2,j}, \dots, P_{i_0+n,j}$, is obtained from Eq. (D6), truncated to the n leading terms. This relation is best expressed in determinantal form as

$$\begin{vmatrix}
 P_{i_0,j} & r_0^{m+1/2} & r_0^{m+5/2} & \dots & r_0^{m+1/2+2(n-1)} \\
 P_{i_0+1,j} & r_1^{m+1/2} & r_1^{m+5/2} & \dots & r_1^{m+1/2+2(n-1)} \\
 P_{i_0+2,j} & r_2^{m+1/2} & r_2^{m+5/2} & \dots & r_2^{m+1/2+2(n-1)} \\
 \dots & \dots & \dots & \dots & \dots \\
 P_{i_0+n,j} & r_n^{m+1/2} & r_n^{m+5/2} & \dots & r_n^{m+1/2+2(n-1)}
 \end{vmatrix} = 0, \quad (D9)$$

where r_ν is the r value of the row $i=i_0+\nu$. For practical purposes we find that $n=2$ is sufficient. i_0 must not be too large, though, since at points far removed from the axis, the asymptotic expansion is not valid any more. To achieve higher accuracy, we find it useful to work with a smaller h , in the vicinity of $i=i_0$.

³³ See G. Forsythe and W. Wasow, *Finite-Difference Methods for Partial Differential Equations* (Wiley-Interscience, Inc., New York, 1960), p. 201.

Obviously, Eq. (D9) can also be written in the form

$$P_{i_0,j} = \sum_{\nu=1}^n C_\nu P_{i_0+\nu,j} \quad (D10)$$

Inserting these expressions in Eqs. (D7), and arranging all the $P_{i,j}$ of the internal points in a vector \mathbf{P} , our equations can be represented by the matrix equation

$$\mathbf{A}\mathbf{P} = \mathbf{E}\mathbf{P}. \quad (D11)$$

A is a sparse square matrix, of dimension N equal to the number of internal (active) points; it is almost symmetric, except for points close to the boundary, or to where a change of lattice density occur. Whereas the differential equation (D5) has an infinite number of positive eigenvalues, bounded from below but not from above, the matrix equation (D11) has a finite number of eigenvalues $E_1 \leq E_2 \leq \dots \leq E_N$. The lowest eigenvalues, in which we are interested, should provide a better approximation to the corresponding lowest eigenvalues of the original problem. This is, indeed, the case, since they are associated with eigenfunctions with a small number of nodes. In general, when solving for an eigenvalue, the mesh size should be small, compared to the nodal distance of the associated eigenfunction.

Let us now define a family of $N \times N$ -matrix operators $B(\eta)$ by

$$B(\eta)\mathbf{X} = (\mathbf{A}\mathbf{X} - \eta\mathbf{X}) / |\mathbf{A}\mathbf{X} - \eta\mathbf{X}|, \quad (D12)$$

where η is any scalar. Due to the sparseness of A , this operation is suitable for rapid execution on a high-speed electronic computer. Let \mathbf{X} stand for an arbitrary N vector, that can be written as some linear combination of all the eigenvectors Φ_1, \dots, Φ_N of A , i.e.,

$$\mathbf{X} = \sum_{\nu=1}^N C_\nu \Phi_\nu; \quad C_\nu \neq 0 \text{ for all } \nu. \quad (D13)$$

Therefore, operating with $B(\eta)$ on \mathbf{X} will give a normalized vector

$$B(\eta)\mathbf{X} \sim \sum_{\nu=1}^N C_\nu (E_\nu - \eta) \Phi_\nu, \quad (D14)$$

and generally

$$B^n(\eta)\mathbf{X} \sim \sum_{\nu=1}^N C_\nu (E_\nu - \eta)^n \Phi_\nu. \quad (D15)$$

If the eigenvalue E_N is largest in absolute magnitude (which is usually the case for physical problems), we can utilize the following set of relations:

$$\lim_{n \rightarrow \infty} B(0)^n \mathbf{X} = \Phi_N, \quad (D16)$$

$$\lim_{n \rightarrow \infty} B(E_N)^n \mathbf{X} = \Phi_1, \quad (D17)$$

$$\lim_{n \rightarrow \infty} (B(E_N)^\lambda B(E_1))^n \mathbf{X} = \Phi_2 \text{ for any } \lambda. \quad (D18)$$

TABLE VIII. The Coulomb energy of a sphere of unit radius and total unit charge for different values of mesh size δ . The value obtained by extrapolation to zero mesh size is also given. The exact value is 0.6.

δ	1/16	1/32	1/64	0 (Extrapol)	Exact
E	0.5648	0.5875	0.5968	0.5996	0.6

Since operating by $B(E_\nu)$ on any vector will ideally eliminate the component Φ_ν in it, we can generalize Eqs. (D16), (D17), and (D18) and write

$$\lim_{n \rightarrow \infty} [B(E_N)^\lambda \prod_{\alpha=1}^{\nu} B(E_\alpha)^{\lambda_\alpha}]^n \mathbf{X} = \Phi_{\nu+1}. \quad (\text{D19})$$

The necessity of operating with each $B(E_\alpha)$, $\alpha = 1, \dots, \nu$ many times, when solving for $\Phi_{\nu+1}$ stems from the fact that $E_1 \dots E_\nu$ are known only approximately. The closer E_α to its actual value, the lower need λ_α be in comparison with λ . It is possible in practice to devise criteria for the relative application of the various $B(E_\alpha)$. However, for all small α , we also have

$$\lim_{n \rightarrow \infty} B(E_\alpha)^n = \Phi_N. \quad (\text{D20})$$

The inaccuracies in the first eigenvalues, will therefore put a limit on the number of different eigenvalues that can be found for each m . In our computations we use the Control Data Corporation 6600 computer,³⁴ with a precision of about 17 decimal figures, where we find, owing to the above consideration, a limit of about 12 eigenvalues that can be computed for each value of m .

APPENDIX E: ACCURACY OF CALCULATIONS

In this Appendix we deal with questions relating to the accuracy of the calculations reported in the text.

³⁴The calculations were performed at the Atomic Energy Commission Computing and Applied Mathematics Center, Courant Institute of Mathematical Sciences, New York University. Earlier computations were executed on a CDC 1604A computer at the Weizmann Institute of Science, Rehovot, Israel.

These divided into two basically different parts: Evaluation of single-particle energies and computation of Coulomb self-energy integrals. Both are further combined to generate the potential energy surfaces whose properties (and in particular the SP shapes) are investigated.

Accuracy is basically achieved and controlled by a procedure of successive refinements of the grid, as described in Appendix D, and extrapolating hyperbolically to zero mesh size. An example for such a procedure, which illustrates the dependence of the calculated eigenvalues on their quantum numbers and the grid fineness, is given in Table VI. The extrapolated values are also quoted. We note the eventual deterioration of the quality of the calculation with the increase of the principal quantum number. Nevertheless, we note that *differences* between related eigenvalues are reproduced better than the eigenvalues themselves.

As a test case for which all the exact eigenvalues are known precisely independently, we take the sphere. In Table VII, we give the exact eigenvalues under the nl column, and the calculated ones under their respective magnetic quantum numbers.

The Coulomb self-energy was calculated using the disc-disc interaction method. Again the spherical test-case results, which are summarized in Table VIII, point to the same magnitude of over-all accuracy, which is slightly better than one part in a thousand.

The determination of coordinates of SP shapes was essentially done through employing the perturbation technique described in the text on previously calculated results. Generally speaking, because of the specific motivation regarding asymmetry, we have relatively accurate results only for the asymmetry measuring parameter. We have tried to indicate the degree of inaccuracy in the figures throughout the text, although these are only rough estimates.

ACKNOWLEDGMENT

We wish to thank Professor W. J. Swiatecki for many helpful and interesting suggestions and discussions.